Carbon dating of agricultural soils and further understanding the transport of CO_2 gas using isotopes

David Zal, MSc candidate

Thesis submitted to the University of Ottawa in partial fulfillment of the requirements for the Master of Science, Earth Sciences

Department of Earth and Environmental Sciences, Faculty of Science
University of Ottawa

© David Zal, Ottawa, Canada, 2023

Abstract:

CO_2 is a greenhouse gas which is significantly emitted by agricultural soils through the decomposition of plant residue and soil organic carbon. Carbon isotopes can be used in determining the source of the CO_2, origin of the carbon, and the age of the CO_2 emissions. This study investigates the transport of CO_2 gas through agricultural soils using carbon isotopes ^{14}C and ^{13}C to complement concentration and production rate measurements in two comparative agricultural settings in Eastern Ontario, one of which has been modified by clearing and dredging of the adjacent riparian zone and one left undredged. Traditional radiocarbon dating measures time through loss by decay, while recent dating is based on matching measurements with the atmospheric $^{14}CO_2$ signal ($F^{14}C$) generated by nuclear bomb testing in the 1950s and 1960s.

CO_2 emissions were analyzed from soil core sections together with soil-probe gas samples and surface flux chamber samples collected from the study area. Soil cores were collected from 0-90 cm at 7.5 cm increments and placed into IsoJar® microcosms for a period of one month. CO_2 in-growth was monitored to provide production rates and samples for ^{14}C and ^{13}C analysis. The radiocarbon data for the microcosms showed that values increase with depth from the current fraction modern value of 1.00 $F^{14}C$ at the surface to an attenuated peak of 1.04 $F^{14}C$ at a depth of 30 to 40 cm and then decrease to values below 1.00 $F^{14}C$. The data collected from the soil-probe gas showed a significant depletion in comparison to the microcosms and the surface chambers. The soil cores were subsequently analyzed by a selective leach oxidation protocol to sample decreasingly labile solid organic carbon. This involved placing the weighed soil samples into MilliQ water for 24 hours, before being passed through two sieves, 63 microns and 0.45 microns. The DOC leachate was collected and analyzed for ^{14}C and ^{13}C. The two solid soil fractions were then dried, treated with HCl to remove carbonate and then oxidized under vacuum with 5% H_2O_2 yielding CO_2 and residual soil carbon for ^{14}C and ^{13}C.

The radiocarbon analysis of these variously labile fractions, together with the microcosm and soil probe measurements, demonstrate that surface emissions at both sites are greatly dominated by CO_2 from recently-sequestered labile organic carbon from the upper 30 cm with minor contribution from earlier, bomb-pulse carbon or from deeper pre-bomb carbon. No significant difference in age of emissions between the dredged and undredged sites was found.

Acknowledgements:

I would like to thank my supervising professor Ian Clark, for his continued support with this project and for the guidance that he has provided during the last three years, particularly, for introducing me to the world of isotopes and his patience in answering my many questions.

I would also like to thank Dr. David Lapen for his insights and pointers on how to further improve the project within the larger Agriculture Greenhouse Gap Program (AGGP) project, as well as extend my thank you to Emilia Craivan for her ongoing support with the field practices.

I would like to extend a thank you to the Jan Veizer lab team, Paul, Kerry, Wendy and Erin for their great insights, vast technical knowledge, and the many laughs we shared.

I would also like to thank the Radiocarbon team for their help in completing this project. I would like to especially thank Jennifer Walker for her many hours spent helping me progress in this project. Without her help and her insight, this project would not have turned out as well as it did. I also would like to thank Professor Brett Walker for allowing me to use his lab to analyse my samples and obtain my final data.

I would also like to thank my friends and family for the support that they have given over these past few years. I wanted to especially thank Angelina for all her help and for listening to all my ramblings about my most recent insights, misconceptions, and eventual corrections.

Finally, I would like to dedicate this work to my late mother Astrid Ginette Spies. Thank you for going through my entire thesis and asking every question under the sun.

Table of Contents

Table 1. Acronyms

Acronyms	Definition
AGGP	Agriculture Greenhouse Gas Program
BP	Before Present
C3	Carbon 13 signature of plants like soy beans
C4	Carbon 13 signature of plants like corn
DOC	Dissolved Organic Carbon
$F^{14}C$	Fraction modern carbon
Fm	Fraction modern carbon
GHG	Green House Gases
OC	Organic Carbon
Oxidation Coarse fraction	Oxidized organic carbon coarse fraction– greater than 60 microns
Oxidation Fine fraction	Oxidized organic carbon fine fraction from 0.45 microns – 60 microns
RC	Recalcitrant Carbon
Recalcitrant Coarse fraction	Recalcitrant organic carbon fraction from 60 microns – greater than 60 microns
Recalcitrant Fine fraction	Recalcitrant organic carbon fraction from 0.45 microns – 60 microns
SOC	Soil Organic Carbon

Introduction

There is currently a significant strain on the environment due to an increased demand on agricultural fields to maintain fresh crop production to sustain the continuously growing population (Janzen, 2004; Zhang, 2022). Not only do these agricultural fields put a significant strain on the environment by causing soil acidification and water eutrophication, but they also contribute immensely to the production of greenhouse gasses (GHG) (Adewale, 2019; Cui, 2013; Yu, 2019). Because of these adverse effects on the environment from the increased use of agricultural fields, focusing more attention on understanding how soils behave has become of greater importance (Ahrens, 2015). This leads researchers to study soil profiles' which emphasizes the change in biological, chemical and physical properties as these change with increasing depth (Hartemink, 2019). Studying these three properties of the soil profile raises the importance of understanding the distribution of soil organic carbon (SOC) because of the increased use of agricultural soils (Zhang, 2022; Jobbagy, 2000). Studies have shown that agricultural fields are depleted in soil organic carbon (SOC) in comparison to soils that have a natural cover of vegetation (Poeplau, 2015). A study that was mentioned in the article of Poeplau, 2015 by Wiesmeier et al. (2013) dives further into the detail of how agriculture fields are depleted in comparison to soils that have natural vegetation cover. Fields that have been used extensively for agricultural purposes demonstrate a depletion of 30-40% SOC in comparison to natural or semi-natural vegetation plots (Don, 2011). This makes areas that have been used or are being used for agriculture, great potential sinks for GHG such as CO_2 (Poeplau, 2015). GHG have a significant impact on the overall global temperature, therefore finding site such as agriculture fields that can be potential sinks for these GHG further raises the point of the importance of needing to understand movement of SOC through the soil profiles. By having a better understanding of the behavior of SOC will help determine if these areas (agricultural fields) can be converted into sinks for GHG, instead of contributing GHG to the atmosphere (Adewale, 2019; Janzen, 2004). Therefore, it is important to get a deeper understanding of how SOC behaves in these profiles, which is possible by using isotopes such as the radioisotope carbon 14 and the stable isotope carbon 13 (Ahrens, 2015; Rheman,2022).

This study was done as part of a larger study that began in 2017 and which included the agriculture greenhouse gas program (AGGP) the University of Waterloo, the University of Carleton and the University of British Columbia. The purpose of the AGGP was to improve the understanding of the agricultural technologies and beneficial management practices that can be adopted by farmers (AFFC, 2021). This specific study took place in Eastern Ontario, close to St-Albert, where the following three locations were surveyed; Field site 10, Field site 1 and Control Forest site. At the two field sites, tile drain systems were installed which were used to regulate the water content in the soil. The tile drains were installed in 10-meter increments from one another, at a depth of 1 meter, and 15 meters from the transition zone/ riparian zone. While this study was conducted, corn was grown during sample collection of 2019, while soy was grown the following year of 2020. The study site on which sample collection was conducted resides on Bainsville soil (Wicklund & Richards, 1962a) which is primarily composed of clay, silt and sand (Government of Canada, 2019). At study site 1, the riparian zone was dredged in 2018 prior to sampling. The soil from the dredged riparian zone was deposited on the transition zone which is between the riparian zone and

field, as seen in Figure 1. The dredging was done to see the environmental impact and to further understand if the load of nutrients that is being released would have a negative effect on the environment post dredging. As previously mentioned, this study was part of a larger program and as such, pervious measurements of the soil age had been determined, which resulted in the results shown in Table 2 below. Table 2 demonstrates that the topsoil horizon of 50 cm is modern for the transition zone, while field and at depth has an older radiocarbon signature (AFFC, 2021; Orekhov (2017)).

Table 2. Age of soils located at study location (table was modified from original), Orekhov (2017)

Material	*Location*	*Depth (cm)*	*$F^{14}C$*	*+-*	*Age (BP)*
Soil	Transition zone	10	0.9877	0.005	100
Soil	Transition zone	50	0.8496	0.0044	1310
Soil	Transition zone	90	0.5367	0.0048	4999
Soil	Field	10	0.9098	0.0017	760
Soil	Field	50	0.6777	0.0046	3125

Figure 1. Image of study site location; image on the left is study site 10 and image on the right is study site 1. Images were taken in 2019, 1 year after dredging of site 1.

Carbon 14 dating and relevancy:

With the help of isotopes such as carbon 13 (^{13}C) and radiocarbon (^{14}C) which both occur in nature, they can be used to better understand the tendency of SOC in through the soil horizon (Slessarev, 2020). The production of ^{14}C occurs naturally in the stratosphere and then via the carbon cycle moves through the different terrestrial and marine reservoirs. Between the early 1950s to 1963 there was an increased production of ^{14}C due to atomic weapons testing (Clark, 2015; Hua et al., 2013; McNeely, 1994). The weapons testing occurred in the upper atmosphere which resulted in the elevated ^{14}C concentrations seen in Figure 2.

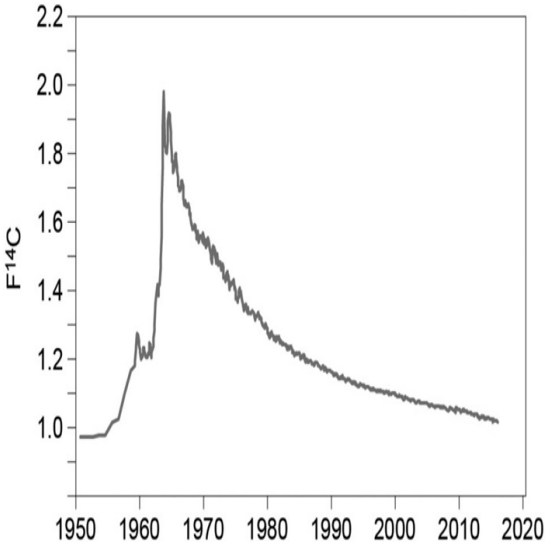

Figure 2. Atmospheric CO_2 radiocarbon activities from 1950 to 2012 AD (Hua et al., 2013) 2012 to 2016 AD (Hammer & Levin, 2017), and 2017 to 2018 AD (new data). $F^{14}C$, fraction modern C.

The industrial revolution brought on a 200-year period of ambiguity prior to the atomic weapons testing because of the sudden increase in burning fossil fuels (Keeling, 1979). The cause of this ambiguity was the burning of coal during the industrial revolution which increased the amount of naturally occurring ^{12}C in the atmosphere which in-turn caused an increasing dilution of the atmospheric ^{14}C ratio, at a rate equivalent to its radioactive decay (Keeling, 1979; Tans et al., 1979). Prior to the ban of atmospheric testing of thermonuclear weapons, the testing that occurred during the 1950 to 1963 resulted in a twofold increase in $F^{14}C$ of atmospheric CO_2 (Figure 2; Clark, 2015; Hua et al., 2013; McNeely, 1994). This rapid increase of $F^{14}C$ in the atmosphere declined over time with the exchange though terrestrial and marine carbon reservoirs (Hua et al., 2013; Reimer et al.,2004) and the continuous burning of fossil fuels (Graven, 2015). Carbon dioxide from the atmosphere gets incorporated into the terrestrial ecosystems and biosphere via the carbon cycle which can be used in soil carbon studies (Blume et al., 2022). When measuring ^{14}C, a ratio between ^{14}C to ^{12}C is used, and this ratio is then normalized as fraction of modern carbon. This ratio can be expressed as a fraction of modern carbon, or $F^{14}C$, which decreases through radioactive decay with a half-life of 5730 years, making it a remarkable tool to date the past 50,000 years (Keeling,1979). The novel use of ^{14}C from the bomb-pulse for soil studies is very helpful in understanding the age of recently sequestered carbon released as CO_2 that is being respired out of the soils.

Soil Organic Carbon pools:

There is an increasing interest in understanding how SOC behaves and interacts throughout the soil profile. We know that SOC is made up of different components, which can be characterized by chemical and physical makeup (Poeplau et al., 2013). As stated by Zimmerman et al. 2007, soil samples can be separated into fractions that are either (i) easily decomposable, (ii) stabilized by physical-chemical mechanisms or (iii) biochemically recalcitrant. These can be alternatively described as dissolved organic carbon (DOC), organic carbon (OC) and finally recalcitrant carbon

(RC) (Miller et al., 2019; Poeplau et al., 2013). Interest in these three main soil categories has increased over the recent years and resulted in various methods being proposed to separate the SOC into their distinctive fractions (Miller et al., 2019). The primary objective of these methods was to provide a clearer picture of how each of these fractions contribute to the overall SOC content and in turn provide a better estimate to calculate residence time/ turn over time (Zimmerman et al., 2007). Further studies have been performed to improve existing methods to separate the different fractions (Schlutz et al., 1999). The application of looking at the different carbon pool fractions for this project is to determine the age of each these fractions since DOC, OC and RC each behave differently to one another and therefore will yield a different isotopic value when analyzed. This in turn will provide a better understanding of the ages of different fractions that are observed in SOC.

Objectives/hypothesis:

The goal of this study is to determine the age of the GHG CO_2 that is being respired from farm fields and their adjacent riparian zones. Additionally, it is to create an age-depth profile for each site showing the relative age of each SOC that is present in these soils. This study will also focus on determining the age of each soil organic carbon fraction and how this impacts the overall perceived age of the SOC in the soil. Additionally, a mass balance will be used to verify if the method that was used to separate the organic carbon pool fraction was successful or not. It is anticipated that the overall results of this project will result in a relative modern fraction of carbon and that the general trend of these depth profiles will indicate a shift from a modern to a more radiocarbon dead fraction. It is also anticipated that the DOC fraction will largely contribute to the overall age of the SOC.

Materials and Methods

Study site:

The study site was located outside of St. Albert on Concession Rd 8 where field sites 1 and 10 are situated (Figure 3). The forest site was located at Concession Rd 7, approximately 50 kilometres outside of the City of Ottawa. The farm fields that were chosen for the study sites were owned by independent farmers, however since the government program was being led by Agricultural Canada, our team was permitted to sample these fields. There was a total of 14 study sites, however this paper will only be focusing on the following sites;

- Field site 1 including the riparian zone,
- Field site 10 including the riparian zone and,
- A forest site used as the control site.

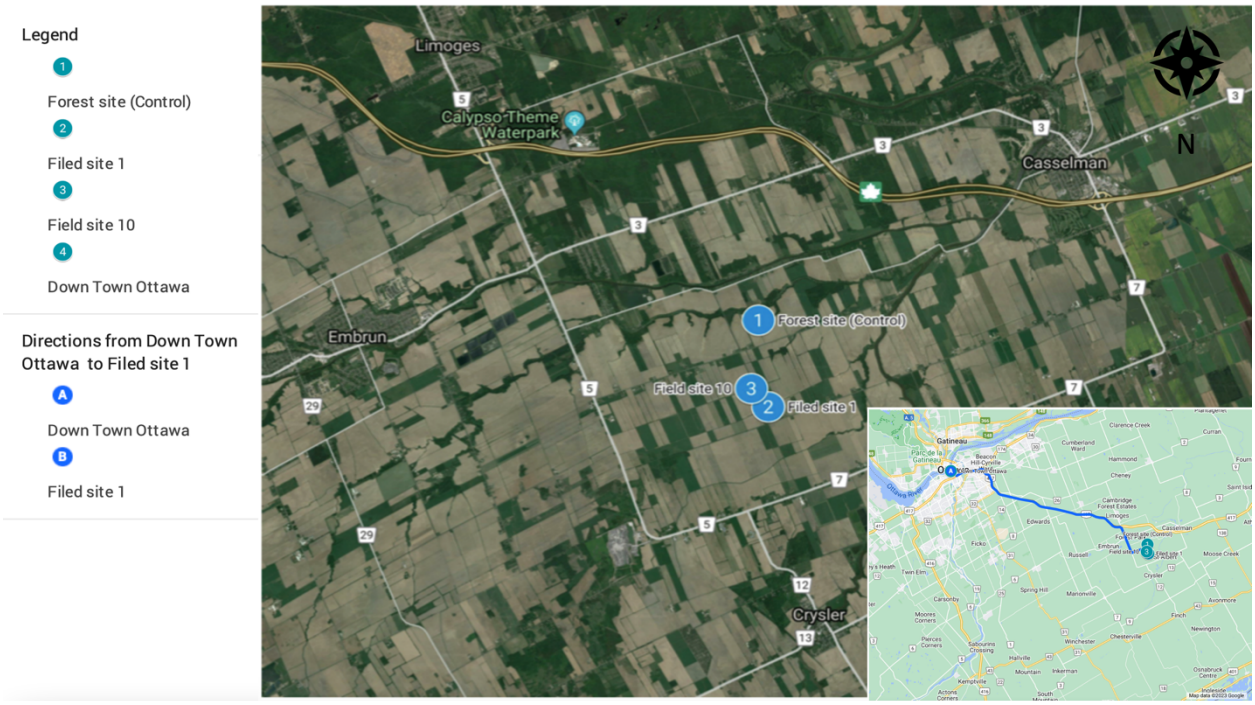

Figure 3. Map of study sites with locations indicated

Field site 1 riparian zone was chosen as it had been dredged, while field site 10 riparian zone was chosen as it had not been dredged. Since field site 1 and field site 10 were located approximately 2 kilometers apart, this allowed for a local comparison of both sites. The control site was located further away and having not been altered by farming, it was the ideal control site for this study, compared to field sites 1 and 10 as they were altered by farming on an annual basis. This provided a contrast between data collected across all the study sites and allowed for further interpretation of what was occurring isotopically.

Soil core collection:

The following materials were required for soil core collection: a hollow stainless-steel pipe with a diameter of around 7.5 cm, a sludge hammer, a wooden disk, a long wooden rod, steel wire and a flat piece of wood.

Figure 4. Materials used for soil core collection: 1 sludge hammer, 2 wooden rods, 3 stainless-steel pipes (7.5 cm diameter), 4 wooden disks.

The soil core collection was completed by using the stainless-steel pipe as seen in Figure 4 and placed in the desired location, with the wooden disk inside the pipe. A piece of wood was then placed on top of the pipe, before using a sledge hammer to hammer the pipe into the ground. Prior to hammering the pipe into the ground, the pipe was marked with 7.5 centimeter (cm) increments spanning up to 90 cm. The pipe was then hammered into the ground up to 15 cm in depth, before being pulled out. After the pipe had been pulled out of the soil, the wooden rod was inserted into the pipe and then used to help remove the soil core from the pipe. The soil core was then cut into pieces with a length of 7.5 cm and then placed immediately into a gas-tight container with a septum-fitted lid (IsoJar™ from Isotech Labs). It is important to note that the soil core that was collected initially was the soil core that spanned between 7.5 to 15 cm, while the remaining soil cores spanned between 0 to 7.5 cm. This process was repeated until 90 cm of soil core was extracted from the study location and repeated for both field sites 1 and 10, where two additional

locations were also sampled; Shoulder site and Bank (riparian) site. For control site Forest, only 1 depth profile of 0 to 90 cm was collected.

IsoJars:

After the completion of soil core sampling, the IsoJars were returned to the lab and left to incubate for a period 3 to 4 weeks. The IsoJars were monitored for oxygen levels and ingrowth of carbon dioxide levels over several weeks. The monitoring of the oxygen levels and carbon dioxide levels was done using an SRI GC (Gas chromatograph) on a weekly basis to determine when the gases in the overlying headspace had reached plateau. Once the plateau has been reached, the carbon dioxide gas was extracted from the IsoJars' headspace and purified. This was done using a multipurpose line following the standard operating procedure provided by the AEL Lalonde Radiocarbon Lab. The purified carbon dioxide gas was then trapped and sealed in a break seal, which was used to further process the gas into graphite and then analyzed on the Accelerator Mass Spectrometer (AMS) for Carbon 14. In addition to the Carbon 14 analysis, a small sub sample was taken prior to sealing the carbon dioxide in the break seal, which would later be analyzed for Carbon 13.

Gas probes:

Gas probes (1/4" ID stainless steel tubes with gas intake hole in sidewall) were installed 1 meter away from the soil core location and used to extract free gas from specific soil depths. The gas probes were installed at 7.5 cm and 30 cm, and then in 15 cm increments until a depth of 90 cm was reached. Gas probes were installed at both field sites 1 and 10 field, transition zone and riparian zone. They were also installed at the forest control site following the same depth intervals. The gas probes were left to settle for a week before sampling. The sampling was done by using a pre-evacuated 500 ml Wheaton bottle which was evacuated to a vacuum of 60 millitorr. Using a syringe with a 3-way valve attached and an additional longer piece of Tygon^{TM} tubing with one end attached to the 3-way valve and the other end placed over the gas probe. Once this set up had been attached, the tubing was cleared by evacuating the gas probe three times to ensure no atmospheric contamination would occur. Next, the needle was inserted into the pre-evacuated Wheaton bottle and gas was pushed out of the syringe. After the needle had pierced the septa, the 3-way valve was turned to allow the gas flow directly into the pre-evacuated Wheaton bottle. Once the Wheaton bottle was fully equilibrated, it was then over pressured by around 120 ml. This was done to allow sub sample collection in the lab and to ensure an accurate reading of the concentration of the carbon dioxide in the Wheaton bottle. This process was repeated for each individual gas probe. Once the concentration of carbon dioxide had been determined in the Wheaton bottle, the gas inside the Wheaton bottle was extracted using a multipurpose line. The carbon dioxide gas was then purified and sealed in a break seal. The purified carbon dioxide gas was then analyzed for Carbon 13 and Carbon 14 isotopic signature.

Surface gas flux chambers:

The gas flux chambers were installed 1 meter from the soil core extraction site. The chamber was of 40 cm length and 60 cm diameter PCB piping, hammered into the ground to a depth of around 10 cm, leaving 30 cm above ground. The chambers were hammered in using a mallet as to not damage the surface of the piping, as the surface was used to create a seal with the lid that was attached to the chamber bottom. The lid was made of PVC with a septum installed in the lid and had a silver reflective foil attached as well as a small exhaust tube to allow for atmospheric pressure inside the chamber. There were three latches attached to the lid that were clipped into the bottom of the chamber which when closed, with the addition of a very soft type of foam, formed an airtight seal. After the installation was completed and the lid had been placed on the chamber, it was left to accumulate the exsolving gas from the soil for 24 hours before sampling. The same method for gas sampling from the gas probes was used for the gas flux chambers, however with a minor modification of using two needles instead of one in order to allow the gas transfer to occur as both septa needed to be pierced. Prior to injecting the needle into the pre-evacuated Wheaton bottle, the tubing was flushed to ensure no atmospheric contamination occurred. The sample was then injected into the Wheaton bottle and left to equilibrate for 5 minutes. Once the Wheaton bottle had fully equilibrated, it was then over pressurized by around 120 ml. This was performed in order to collect a sub sample and obtain the concentration of the carbon dioxide inside the Wheaton bottle. The sample was then subsequently extracted on the multipurpose line and the purified carbon dioxide gas was sealed into a break seal which was later analyzed for Carbon 14 and a sub sample analyzed for Carbon 13.

Gas Analysis SRI Chromatograph:

The carbon dioxide concentration in the samples collected was determined with an SRI Gas chromatograph. A sub sample of 5 ml was injected into the SRI GC inlet port. This specific SRI GC had a 1 ml sample loop with a 1 ml exit loop at the end. The sample flushed the loop 5 times ensuring that only the desired sample remained in the 1 ml sample loop and prevented any back streaming from atmospheric lab air. Once the sample had been injected, the program that ran the SIR GC was started which opened the valve and allowed 0.5 ml of gas into the thermal conductivity detector (TCD) column, with helium acting as the carrier gas and 0.5ml of gas into flame ionization detector column (FID). The TCD column was used to determine the amount of nitrogen, oxygen, carbon dioxide, methane, ethane, propane, butane, and pentane. The FID had similar capabilities, however could only provide concentrations for carbon chains. The advantage of having both a TCD column and an FID, allowed for analysis of samples with very high and low concentrations and the ability to obtain results immediately. The calibration of the machine was done prior to injecting the first sample and done using known reference gases.

Analysis of Soil Organic Carbon Content (SOC):

Soil samples were analyzed for total organic carbon concentration using an elemental analyzer. The soil samples, prior to being weighed and placed into the elemental analyzer, were treated with hydrochloric acid (HCl) and then subsequently washed with deionized water to remove carbonate minerals. The process of treating the soil samples with HCl was done by placing the samples into a fume hood and adding diluted HCl with a concentration of 10% to each sample, while ensuring that the samples were covered and placed on a hot plate to accelerate the reaction. This treatment was performed three times to ensure that all inorganic carbon had been removed from the soil samples. The samples were then rinsed with deionized water and dried. Once the samples were dried, they were weighed and placed into the elemental analyzer. The elemental analyzer used flash combustion to instantaneously combust all samples and converted them into CO_2. To accelerate this reaction, tungsten oxide was added to each sample to ensure complete combustion. The gas was then brought to the detector and the concentrations were written down to be used for further analysis.

Carbon pool separation:

The organic carbon for each soil sample was subdivided into five specific pools of carbon, by water leach, size fractionation by sieving and reactivity fractionation by partial oxidation. The separation by size used 60 microns and 0.45 microns. These were then classified as (i) DOC representing dissolved organic carbon passing the 0.45 microns filter paper, (ii) soil fraction between 0.45 and 60 microns, and (iii) soil fraction greater than 60 microns in size.

DOC leach and Size Fractionation:

The dissolved organic carbon fraction (labile fraction) was separated from the soil core by the following procedure; the soil core was split into two aliquots, one of these aliquots was used for the dissolved organic carbon (DOC) leach while the other was used for incubation using an IsoJar. The aliquot that was used for the DOC leach was placed in a 500 ml beaker which was pre-baked at 450°C for 8 hours to ensure that there were no residual carbon sources left on the beaker that may contaminate the sample (AEL, 2020). The beaker was then weighed, and its mass was recorded. The soil aliquot was then weighed into the beaker and the mass was again recorded. Following the last step, 300 grams of Milli-Q water was added into the beaker. This process of weighing and water addition were repeated for all other aliquot samples. The newly filled beaker was then placed into a sonicator and left for 30 minutes to ensure that the soil core would separate, and allow the surfaces of the grains to interact with the surrounding water, allowing for a faster equilibrium to be reached in the leaching process. The solution mixture was left to sit for 24 hours allowing for the DOC to be leached out of the soil (Peoplau, 2013). After the 24-hour period, the sample was placed again into the sonicator and sonicated for 30 minutes. The soil water solution was then passed through a 60-micron sized sieve into a 1-liter beaker which was baked at 480°C. Prior to passing the new solution through the 0.45-micron size filter, it was centrifuged using 100 ml wide mouth bottle in order to separate the soil out of solution to avoid blocking the filter (Schultz, 1999). The new solution was then passed through a 0.45-micron size filter, collected and

placed into a pre-baked 500 ml Wheaton bottle. The bottle was then sealed and later treated for further analysis. The soil fractions retained on the 60-micron mesh and on the 0.45-micron filter paper were then collected, dried and prepared for further analysis.

Labile and Recalcitrant Organic Carbon:

The solid soil fractions (>60 μm and 0.45 to 60 μm) that were obtained during the DOC leach process were dried in the oven at 60°C. After the drying process, the samples were moved into a fume hood in which they were treated with 10% hydrochloric acid to remove the inorganic carbon from the soil fractions. This step was repeated until no more reaction was visibly occurring for these soil fractions. The samples were then rinsed with Milli-Q water and then placed into the oven to be dried.

After the removal process of the inorganic carbon was completed, the soil samples were weighed into pre-baked Wheaton bottles. These bottles were then capped with a grey butyl septa. Prior to capping the bottle, the sample was weighed into the bottle targeting 1 – 1.5 grams of soil depending on the organic carbon concentration. The Wheaton bottle with the sample was then flushed with nitrogen gas for 10 minutes to create a carbon dioxide free headspace for the rest of the procedure to avoid any contamination. Next, the Wheaton bottles with the samples were moved to the fume hood in which 20 ml of hydrogen peroxide was added at a concentration of 3.82% and 3 ml of Nitric acid at a concentration of 1% in order to provide a final concentration of 0.1 molar nitric acid in solution. After the addition of both solutions, the bottle with the sample was placed into an oven for 2 hours at 70°C (Schultz, 1999). The samples were then removed from the oven and left to cool overnight. The carbon dioxide gas was then collected using a vacuum line and the sample was sealed in a break seal for further analysis. This entire process was repeated for all carbon dioxide samples. Once the carbon dioxide was removed from the head space in the Wheaton bottle, the soil sample fractions were removed and placed in falcon tubes, where they were rinsed with Milli-Q water and then dried for further analysis.

Closed tube combustion/EA analysis:

The EA method that was used involved samples being weighed into tin capsules for samples that had a high residual carbon concentration. The amount that was weighed into capsules was determined by the concentration left in the soils after treatment. Tungsten oxide was added to these samples to aid with flash combustion. The sample were then combusted using an elemental analyzer and the carbon dioxide gas was trapped and sealed in a break seal.

For the samples that were too low in residual carbon concentration to be used for analysis in the elemental analyzer, an alternative analysis method was used; closed tube combustion. For this method, the soil samples were weighed into quartz tubes and the amount weighed into each quartz tube was determined by how much organic carbon was left in the soil samples. Each sample required the use of 2 to 3 quartz tubes as they had to be split up to ensure that when they would be baked, the quartz tubes would not explode and result in a lost sample. Once the weighing of the samples into the quartz tubes was completed, copper oxide was added into the sample. The quartz tubes were then pumped down on a vacuum line to 8.6e-5 millitorr of pressure and were then subsequently sealed. The addition of the copper oxide was done to allow for the conversion of

organic carbon in the soil into carbon dioxide. Once the quartz tubes were sealed, they were placed into an oven where they were baked at 850°C for 3 hours. This entire process from start to finish took around 15 hours as the oven required time to increase to the desired temperature and then cool down following the same ramping schedule. The samples were then removed from the oven, scored and extracted on a vacuum line where the carbon dioxide was collected and sealed in a break seal.

Multipurpose extraction line:

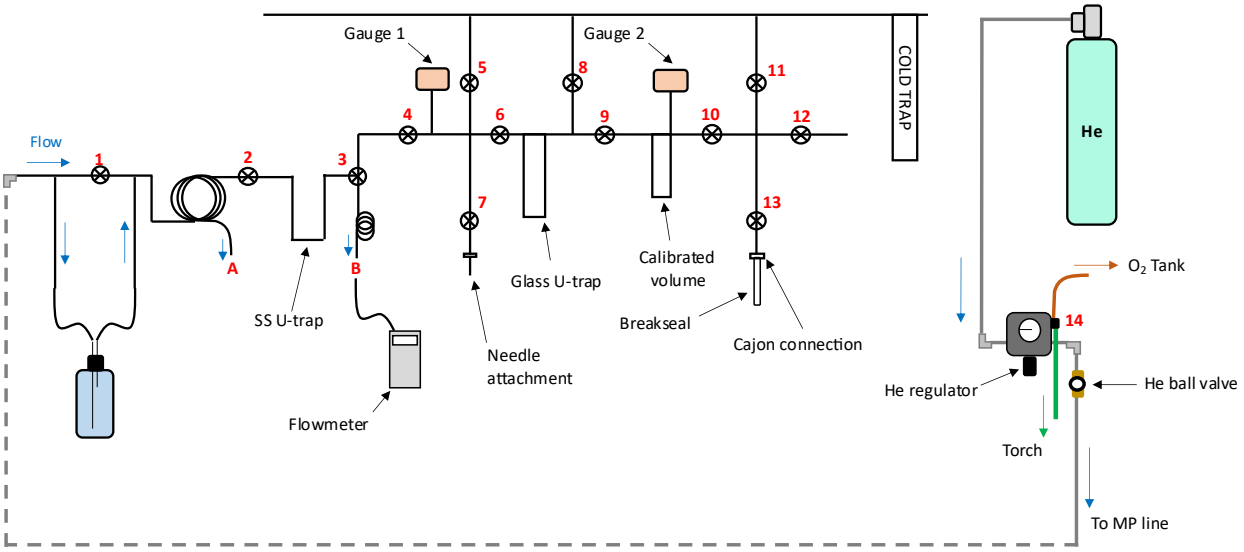

Figure 5. Multipurpose line schematic

A multipurpose vacuum extraction line was used to extract the carbon dioxide gas that was collected and the AEL Radiocarbon lab procedure was used and followed. This line was used for serval different samples ranging from water to pure gas samples. As seen in the schematic of Figure 5, the sample bottle or container was pierced using a needle through a grey butyl septum with two needles, one which was used as the inlet needle which had helium flowing out, and one which was used as the outlet needle in which the gas could escape the sample bottle. The helium sample mixture would travel through a nathion loop that had a venting section (labelled as A in Figure 5). This nathion loop had an inner and outer tube which allowed for a pressure difference to occur preventing the sample from diffusing out while traveling through the loop. The helium sample mixture would then travel to a stainless-steel u-trap which would have a liquid nitrogen dewar placed under it. This would cool the stainless-steel u-trap and allow for the carbon dioxide gas to be trapped. To increase the efficiency of gas trapping, the u-trap was packed with cobalt wool. The gas was then trapped in the u-trap and the excess helium gas was allowed to vent to the atmosphere through the venting loop (labeled B in Figure 5), to which a flow meter was attached to ensure that a proper flow was maintained throughout the entire procedure. After the trapping of the sample was complete, the valve of the venting section was closed off and the sample was then transferred to the next u-trap. Prior to this transfer, any of the excess gasses were pumped away. A water trap was placed on the stainless-steel u-trap while a liquid nitrogen dewar was placed on the glass u-trap. This allowed for the carbon dioxide gas to be transferred from one u-trap to the other and permitted any water to be left behind in the first u-trap. This process was repeated once more and the gas was then transferred to a calibrated and calculated volume, in which it could then be

accurately measured. Once the sample measuring was complete, based on the size of the sample, it was either transferred directly into a break seal or was split into smaller aliquots and then transferred into a break seal. This allowed sample extras to be saved for re-analysis if necessary. Depending on the type of sample used at the inlet section, the sample container was left to purge either 5 or up to 30 minutes. The purge time used for each sample container was determined on the container size and the flow rate since the sample container had to be flushed 10 times to ensure that the entire sample had been flushed out and transferred to the u-trap. Transfers between u-traps took 2 minutes and for the transfer from the u-trap to the break seal also took 2 minutes. The break seal was then sealed off using a propane torch.

Break seal to graphite:

Once the sample had been transferred into the break seal, the break seals were placed into an oven and baked at 200°C for 3 hours. The break seals had silver cobaltous in them which helped remove any impurities that might have been left in the break seal. The break seals were then transferred to the graphitizing machine where they were cracked, allowing for the gas to expand into the finger in which they were cracked. The gas was then transferred into a smaller volume by freezing it down with liquid nitrogen. Once the transfer was complete, the volume was filled with hydrogen gas and an oven was attached to that volume and left to bake at 650°C for 6 hours allowing the carbon dioxide gas to be converted into graphite. Upon completion of this process, the ovens were removed, and samples were left to cool to room temperature. The samples were then pressed into targets and loaded onto the wheel where they were then loaded on the Accelerator Mass Spectrometer.

Data analysis:

All the data analysis that was performed for this project was done using the Microsoft Excel, as the program had all the necessary features required to perform the data analysis. The primary use for Excel was to create the graphs to be able to further interpret the data. Additionally, the following formulas where used for data interpretation.

To calculate the ages of the carbon pools:

Age = -8266 x Ln (Fm/1), which is the standard radiocarbon decay equation

To calculate the percent contribution of each depth to the overall observed $F^{14}C$ signature:

$((\text{Rate of Production} \times F^{14}C_{(\text{depth x})}) / ({}_{(\text{avg})}\text{Rate of Production} \times F^{14}C_{(\text{Gas Flux chamber})}))*100$

Results

CO_2 production rate and organic carbon content:

Figure 6 shows the overall rate of production of CO_2 vs the overall organic carbon concentration of the soil profile for study site 10 and the control site. What can be gathered from this figure is the high production rate associated with high organic carbon concentrations and low production rates associated with low organic carbon content. The same findings were also seen in the paper by Blume et al. 2022. In addition, Figure 6 shows that the shallow depths are the areas with a high production rate and high organic carbon content indicating that these are the most active zones.

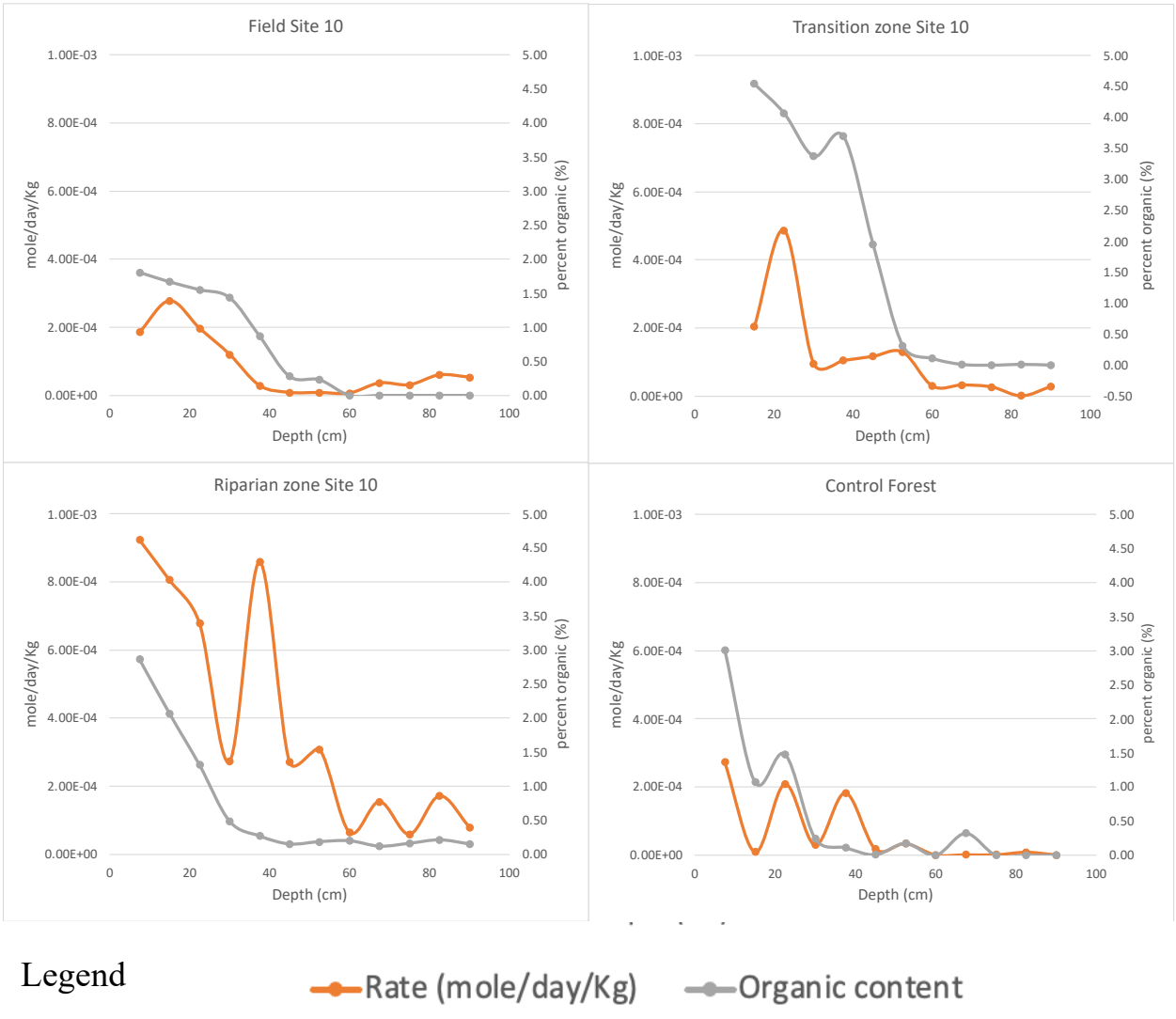

Figure 6. Overall rate of production of CO_2 vs Overall organic carbon content for the soil profiles at study site 10 and the control site. The riparian site was not disturbed the year prior to analysis. This data was obtained by monitoring the CO_2 concentrations from the soil cores in the IsoJar microcosm, over a 6-to-8-week period.

We can assume that most of the organic carbon will be respired out from these zones, which indicates that there would not be much carbon storage occurring in these zones. Based on this information, we can infer that the radiocarbon signature that would be observed from these zones should be primarily modern from the past year or two. In Figure 6, it is observed that for both the filed site and riparian zone there is an increase in the rate of production at depth with low carbon content present, which indicates that there is more activity going at depth and that there might be other driving factors that are increasing the rate of production as it is unlikely originating from the carbon content present.

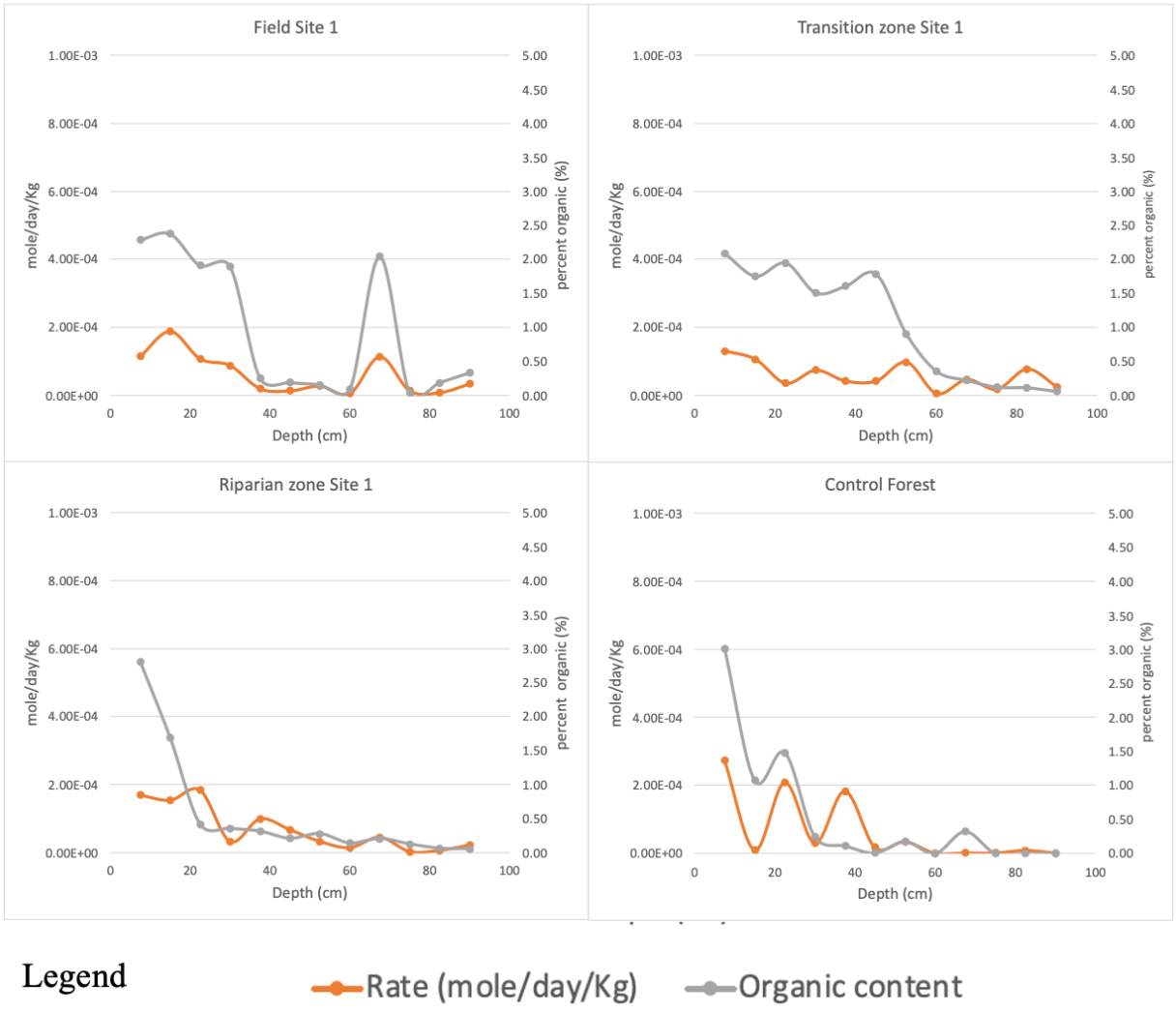

Figure 7. Overall rate of production of CO_2 vs Overall organic carbon content for the soil profiles at study site 1 and the control site. The riparian site was dredged the year prior to analysis. This data was obtained by monitoring the CO_2 concentrations from the soil cores in the IsoJar microcosm, over a 6-to-8-week period.

Figure 7 shows the overall rate of production of CO_2 vs the overall organic carbon concentration of the soil profile for study site 1 and the control site. The trend that is seen in Figure 6 for study site 10 is also observed in Figure 7 for study site 1. The riparian zone at site 1 was previously

disturbed prior to sampling through dredging. We also notice the same type of behaviour as we did at study site 10 with high organic concentrations having high production rates. From what was observed in Figure 6 study site 10, and what is observed from study site 1 in Figure 7, one can infer that the zones with high organic carbon and high production rates will be the most active zones and will be contributing primarily to the overall CO_2 emission from these soils. The general trend appears to be that most of the organic carbon present in the soil is being respired out by metabolic processes. In Figure 7 for field site 1, the organic carbon content has a significant blip in concentration at 67.5 cm followed by an increased rate of production which could originate from another carbon source or an influx of microbial activity which is contributing to the overall production rate for this core.

Both figures 6 and 7 display the control site that was used in this study, which followed the same analytical methods used at study site 10 and 1. A very notable observation that can be made for the control site is that the trend is also represented in study site 10 and 1. Being able to see these trends for both study sites and the control site is very promising because it goes along with the predicted behavior for these sites, which is having high a rate of production and high organic carbon content in the shallow depths and decrease as depth increases. Additionally, it indicates that even though these sites are different from one another, they do not differ significantly in terms of rate of production and organic carbon content throughout the profile. Finally, at these different sites in general, production rate and organic carbon content show a correlation as depth increases.

In Figure 8, we have the ^{13}C depth profile for study site 10 and control site. The graphs shown in Figure 8 depicts an impact of carbonate weathering which can be seen in the gas probe data displayed in both orange and grey. We can also see that there are different impacts of C3 and C4 plants as depth increases. However, we can attribute the depletion that is seen in the gas probes to be primarily from carbonate weathering. This is because the carbonate that is present in the soils originated from a marine source and marine carbon has a ^{13}C signature of 0% (Clark, 2015). As such, the gas probe and gas flux chambers will be impacted by the ^{13}C signature of the carbonates. The evidence that demonstrates impact of carbonate dissolution is the ^{13}C signature obtained from the gas probes which is depleted in comparison to the microcosms and the bulk soil organic carbon. The impact of carbonate weathering is only seen in the gas probes and gas flux chambers and not in the microcosm since the microcosm is a closed system that is not exposed to the environment. As a result of being in an enclosed environment the microcosm mimics the condition from the date of collection. This therefore avoids the impact of carbonate weathering occurring inside of these microcosms.

^{13}C Depth profile:

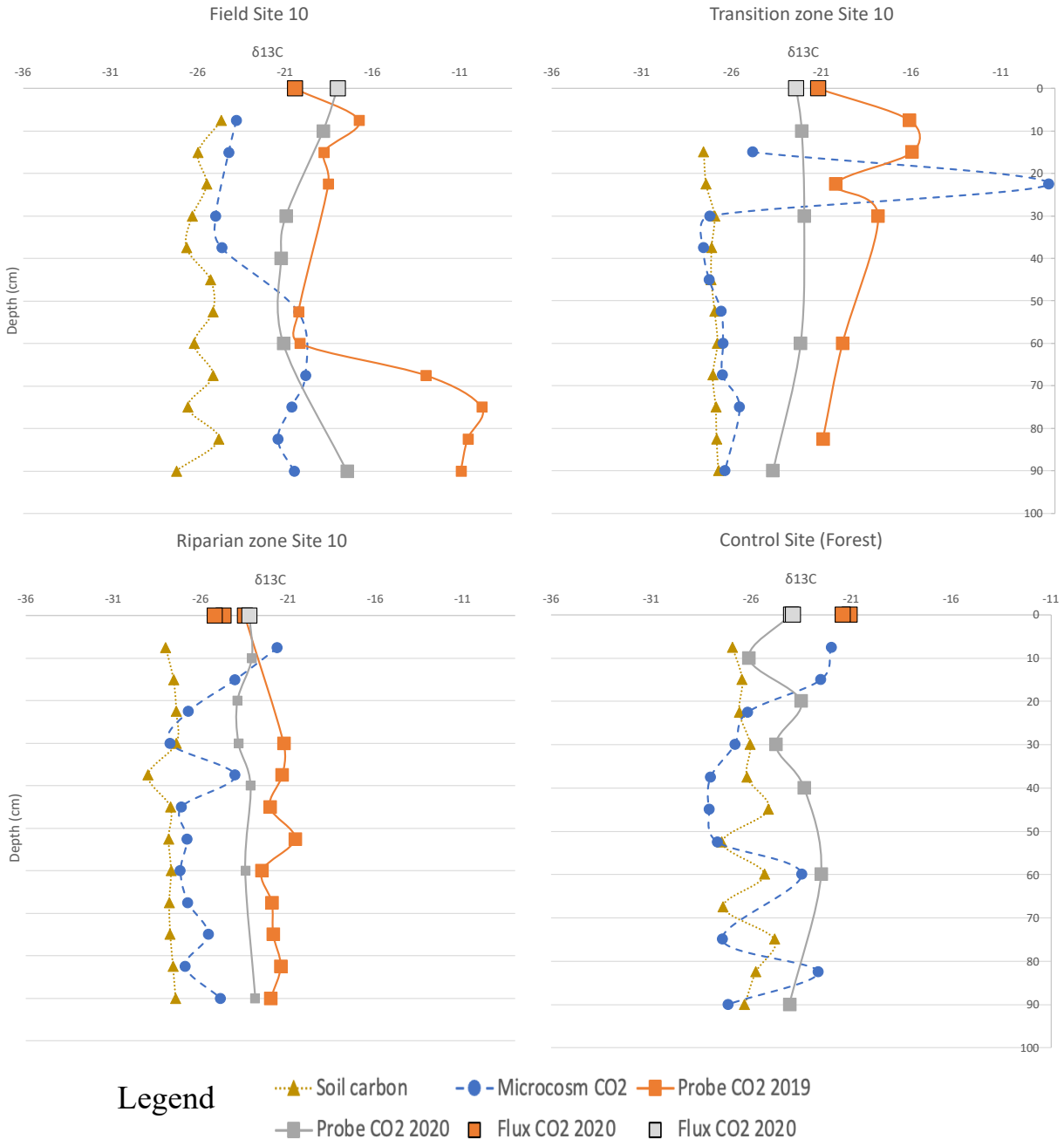

Figure 8. ^{13}C depth profile of study site 10 for Field, Transition zone, Riparian zone and Control site. Plotting Soil Organic carbon, Microcosm, Gas Probes and Gas Flux chambers along a depth profile. The riparian zone was not dredged the year prior to analysis.

In addition, there is an anomaly seen in the data at field site 10 that demonstrates a very rich signature for the gas probe collected in 2019, which is attributed to corn being grown at that site. The observed ^{13}C signature of C4 plants at depth can be attributed through root respiration from the corn plant and through transport facilitated by macropores (worm holes) (Berriel et al., 2016).

The following year the probe sample was collected and the same impact at depth from C4 carbon on the ^{13}C signature was not observed as no corn was grown that year. As such, we can determine that impacts from C4 plants might only be on a seasonal scale. However, we do see that the 2019 and 2020 gas probe data displayed depletion again, and very closely followed the same trend as the probe from 2019, further proving that we have carbonate weathering that is occurring in this system which is impacting the gas probes ^{13}C data. For both Figures 8 and 9, the ^{13}C depth profile for the riparian zone indicates that there is a heavy impact of solely C3 plants based on the ^{13}C signature (Doner et al., 1997).

Overall, the C4 plant impact on the ^{13}C signature can vary depending on if these plants are present or not at these sites. This same trend is also seen in the overall gas respired out of the soil which is displayed in the ^{13}C signatures of the gas flux chambers. In addition, surveying the graphs in tandem demonstrates that the effect of the carbonate weathering on the isotopic data stays consistent throughout the three profiles displayed in Figure 8.

Figure 9 shows the ^{13}C depth profile of study site 1. As mentioned in Figure 8, carbonate weathering also impacted the ^{13}C signatures of gas probes and gas flux chambers. In addition, the primary organic carbon contribution is from C3 plants, with C4 plants only contributing minorly. As previously mentioned, we see that the inorganic carbon dissolution has a significant impact on the ^{13}C signatures that were obtained at this site. We also see that gas probes at this site are still visibly depleted in comparison to the microcosms, showing that there is an effect of carbonate weathering occurring which is impacting the ^{13}C signatures, which is also being displayed in the flux chambers. In Figure 9 for field site 1 starting at a depth of 40 cm, it is seen that both the microcosm and the gas probe in orange were influenced by carbonate weathering. The reason to the observed variation in the microcosm depth profile is likely due to the tilling of the soils and the soil profile having a higher water content during collection which would cause more carbonate dissolution to occur and impact the ^{13}C signature observed.

For the transition zone of study site 1, the microcosm lines up very closely with the soil organic carbon ^{13}C signature; this same trend was also seen at study site 10. For the gas probe, the signature is depleted in comparison to the microcosm. We can assume that this depletion in the gas probe at shallow depths may have originated from carbonate weathering. Finally, a very similar trend to that of Figure 8, in which there is not a significant impact from C4 plants on the microcosm and that gas probes are depleted in carbon 13, in comparison to the microcosm and the soil organic carbon because of carbonate weathering. Based on these results, it is evident that C3 plants took over the re-vegetation of the riparian zone. As mentioned in other figures, a decreasing impact of C4 plants is seen along all the profiles, from the field zone to the riparian zone, and it is seen that the impact of carbonate weathering remains consistent throughout the profiles. When comparing study site 10 and 1, similar trends are displayed wherein both sites demonstrate an impact of

carbonate weathering, indicating that these two sites follow similar trends even though they are physically separated.

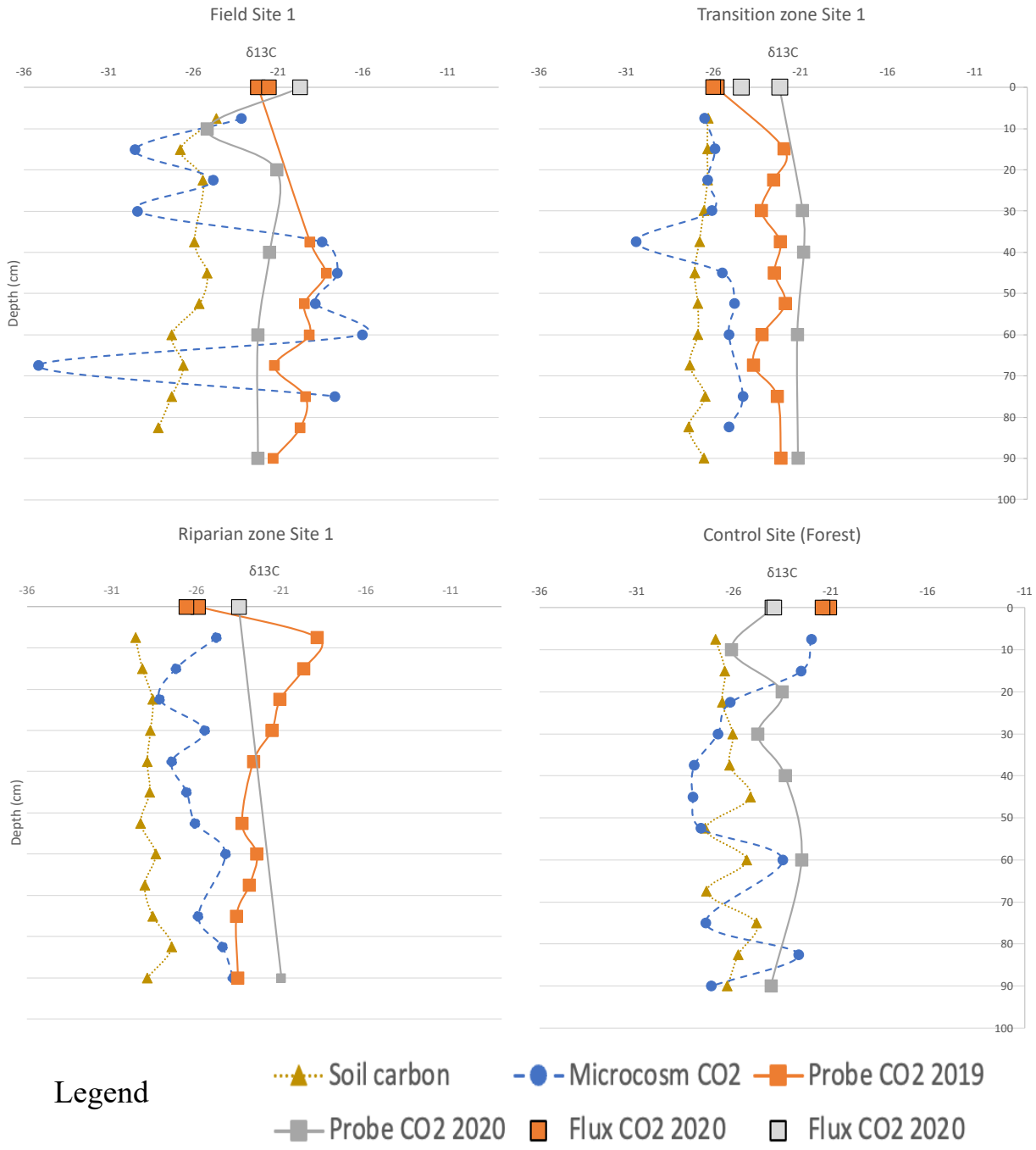

Figure 9. ^{13}C depth profile of study site 1 for Field, Transition zone and Riparian zone and Control site. Plotting Soil Organic carbon, Microcosm, Gas Probes and Gas Flux chambers along a depth profile. The riparian zone was dredged the year prior to analysis.

In both Figures 8 and 9 we have the ^{13}C depth profile for the control site forest. In this depth profile it is observed that there are some minor variations between the microcosm, gas probe and soil organic carbon. However, we do not see a clear distinction between the gas probe and microcosm which would indicate that there was a significant influence from carbonate weathering or other factors as we have seen in the previous two study sites. When comparing the control site to the study sites, see that the trends from study site 10 and 1 line up very well with the control site as these two are very similar to the control site. It is also seen that the riparian zone follows the same trend as the control site with some minor variation. In addition, we also see that the impact of carbonate weathering at this site is not as evident as in the prior study sites. The data indicates that tilling and reworking of the land does not affect the organic pool significantly, however does have a more apparent impact on the carbonate weathering occurring in the system.

With these results we can tell that these study sites do not differ significantly from one another and follow the same trends throughout their profiles. Additionally, the biggest impact to these sites' organic carbon pool is the type of vegetation that is grown as this will impact the type of organic carbon the microbes use for respiration. In addition, the roots also contribute to the organic carbon being respired as shown in the ^{13}C depth profile that was obtained at each site. Finally, the carbonate weathering that occurs throughout these profiles has a significant impact on the ^{13}C data that was obtained for the gas probes, as these are the most sensitive to other environmental factors occurring in the system.

Carbon Pool separation by size and using Radiocarbon:

Figure 10 displays the mass of the main carbon pool of field site 1 (right chart) and their respective radiocarbon activities (left chart). This figure shows how each individual organic carbon fraction found contributes to the overall carbon 14 signature observed in the gas flux chamber. For this specific study, the carbon pools were split into three main categories. These included (i) a dissolved labile fraction DOC (dissolved organic carbon) produced by leaching the soil and filtering to less than 0.45 microns in size, (ii) an oxidize fraction (OC) following an oxidation step using hydrogen peroxide, and finally (iii) a recalcitrant fraction which survived the oxidation step and was combusted for analysis. Prior to the oxidation step, the leached soil was separated into a coarse (>60 microns) and fine fraction (0.45 microns to 60 microns). This was done to determine if separation by size had an impact on the radiocarbon signature observed. The results of this experiment produced the data displayed in Figure 10.

In Figure 10, the Fm carbon values of the individual carbon pools are shown; a Fm value of 1 corresponds to modern current day, a Fm value less than 1 corresponds to an older time period, and a Fm value greater than 1 correspond to carbon originating from the bomb pulse. The variables displayed in Figure 10 at depth of 7.5 cm have their Fm values going from 0.7 to 1.01, from the most recalcitrant fraction to the most labile fraction respectively. As depth increases, the same trend continuous to be observed, which is that the Fm values of each individual fraction decreases with depth. This indicates that as depth increases, the age of carbon in each of these individual pools also increases going from modern up the late Pleistocene (Paul et al., 1997). The age of these different carbon pools range from modern (Fm = 1) to greater than 10,000 years BP. The oldest carbon, at the shallow depth of 7.5 cm, are found in the recalcitrant fractions that were combusted following the oxidation step, which are some 2000 to 3000 years BP. At 75 cm depth, these

fractions are up to 15,000 years BP. Even the oxidized fractions have significant radiocarbon ages from several hundred years to 2000 years BP. This contrasts with the age of CO_2 from respiration in these soils, which is much younger, and in most cases, as shown below, is post-bomb from the past few decades. Bulk carbon in the field profile is less about 1000 years old, with a very minor pool of recalcitrant carbon dating to the late Pleistocene.

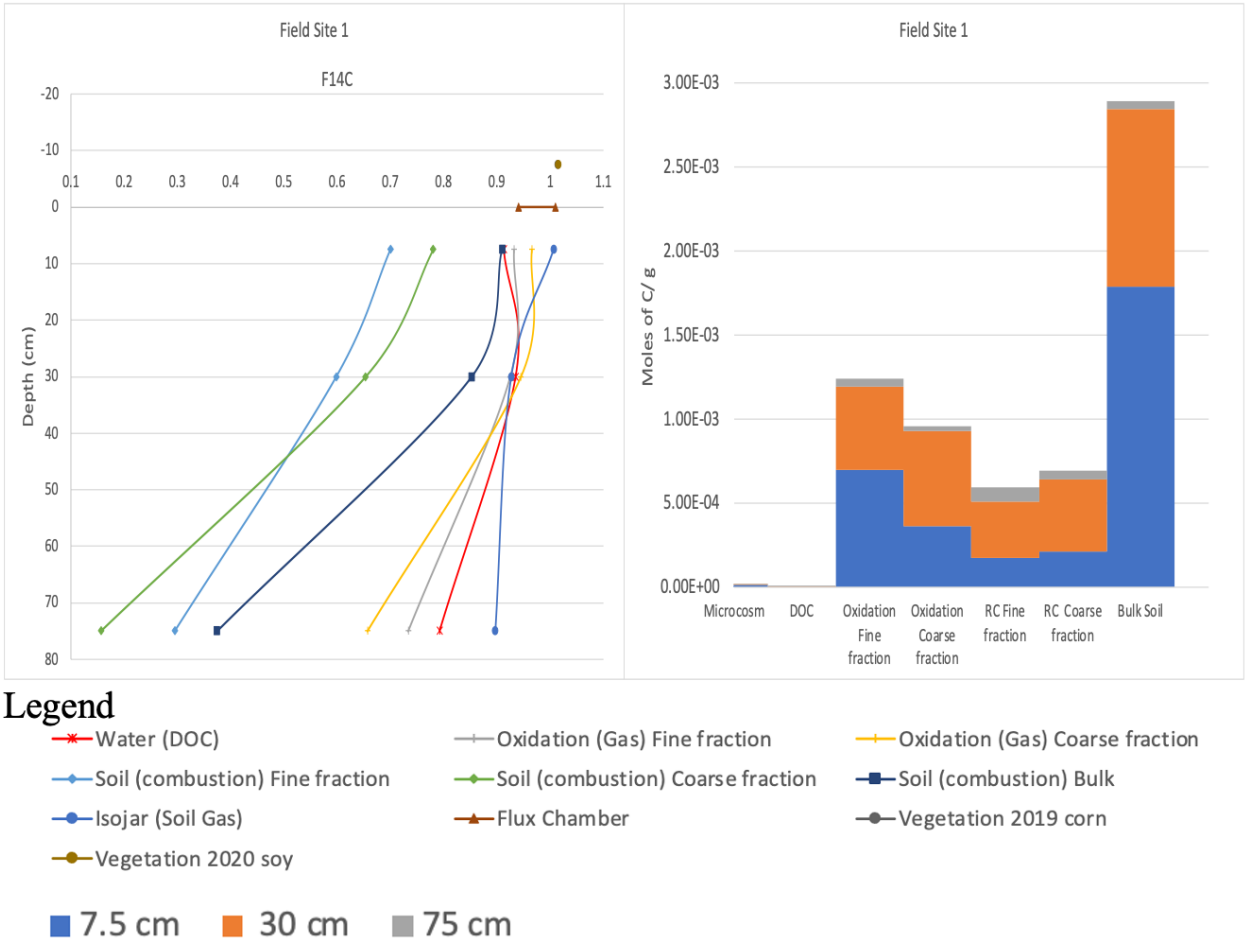

Figure 10. Carbon pool separation of field site 1, was split into the different carbon fractions Liable fraction (DOC, Soil Gas), Organic Fraction (oxidizable fraction) and Recalcitrant fraction (soil combustion). The organic fraction and recalcitrant fractions were split respectively into a coarse fraction (greater than 60 microns) and fine fraction (0.45 microns to 60 microns). The figure on the right hand is displaying the mass of each fraction in comparison to the total bulk soil mass.

Table 3. The different ages of the carbon pool fractions from Figures 10 and 11, which were obtained by taking the Fm values seen in Figures 10 and 11 and converting them into ages using the standard radiocarbon decay equation.

Depth & Location	DOC age (years)	Fine fraction oxidation age (years)	Coarse fraction oxidation age (years)	Fine combustion (RC) age (years)	Coarse combustion (RC) age (years)	IsoJar gas age (years)	Bulk sediment age (years)
Field site 1 7.5 cm	752	568	286	2951	1995	-53	760
Field site 1 30 cm	539	629	458	4129	3425	614	1318
Field site 1 75 cm	1929	2490	3374	9810	14918	879	7898
Forest site 7.5 cm	-408	-226	-432	625	245	-549	5
Forest site 30 cm	1927	2562	879	4962	8806	-319	884
Forest site 75 cm	3586	3472	9227	5822	25945	-438	6879

Table 3 shows the ages for the separate carbon pools at their induvial depths and were calculated using the standard radiocarbon decay equation. The ages with negative values have carbon sources that include post-bomb carbon. This is primarily observed in the IsoJars followed by the oxidation fraction and DOC fraction for the Forest site at 7.5 cm. This indicates that these fractions had a larger amount of post-bomb carbon as their source, resulting in the negative ages obtained. This indicates that each fraction displayed in Table 3 has a different source of carbon as the ages differ significantly. In addition, this demonstrates that microbial respiration is preferentially only going for the youngest and most recently available carbon, as demonstrated in the data for the IsoJars. Overall, Table 3 demonstrates that even though the individual fractions differ significantly from one another in ages, the overall bulk soil age is impacted the most by the oxidized fraction, as also later seen in Figure 16.

The data demonstrates that size fraction does impact the radiocarbon signature, especially for the recalcitrant fraction seen in light blue (fine fraction) and green (coarse fraction) and has minor but still significant impact on the oxidized faction in gray (fine fraction) and yellow (coarse fraction). In addition, we can also see that soil gas (IsoJar) in blue, DOC in red and oxidized fractions in gray and yellow are the primary fractions enriched in radiocarbon. A bulk soil sample was also analyzed and is represented in dark blue, which shows the cumulative soil Fm value of all the organic carbon fractions. As demonstrated in Figure 10, the DOC, both fine and coarse grain fractions of oxidized carbon and soil gas are the main contributors of radiocarbon in the bulk sample, whereas both fine and coarse grain pools of combustion (recalcitrant) carbon are the most depleted in radiocarbon. This is because the oxidized fraction and IsoJar and DOC fractions have the largest amount of mass contribution to the overall bulk soil make up, which is seen in the graph

on the right-hand side for Figure 10. Based on these results it is understood that microbes are primarily using the more liable carbon fractions as their source for respiration.

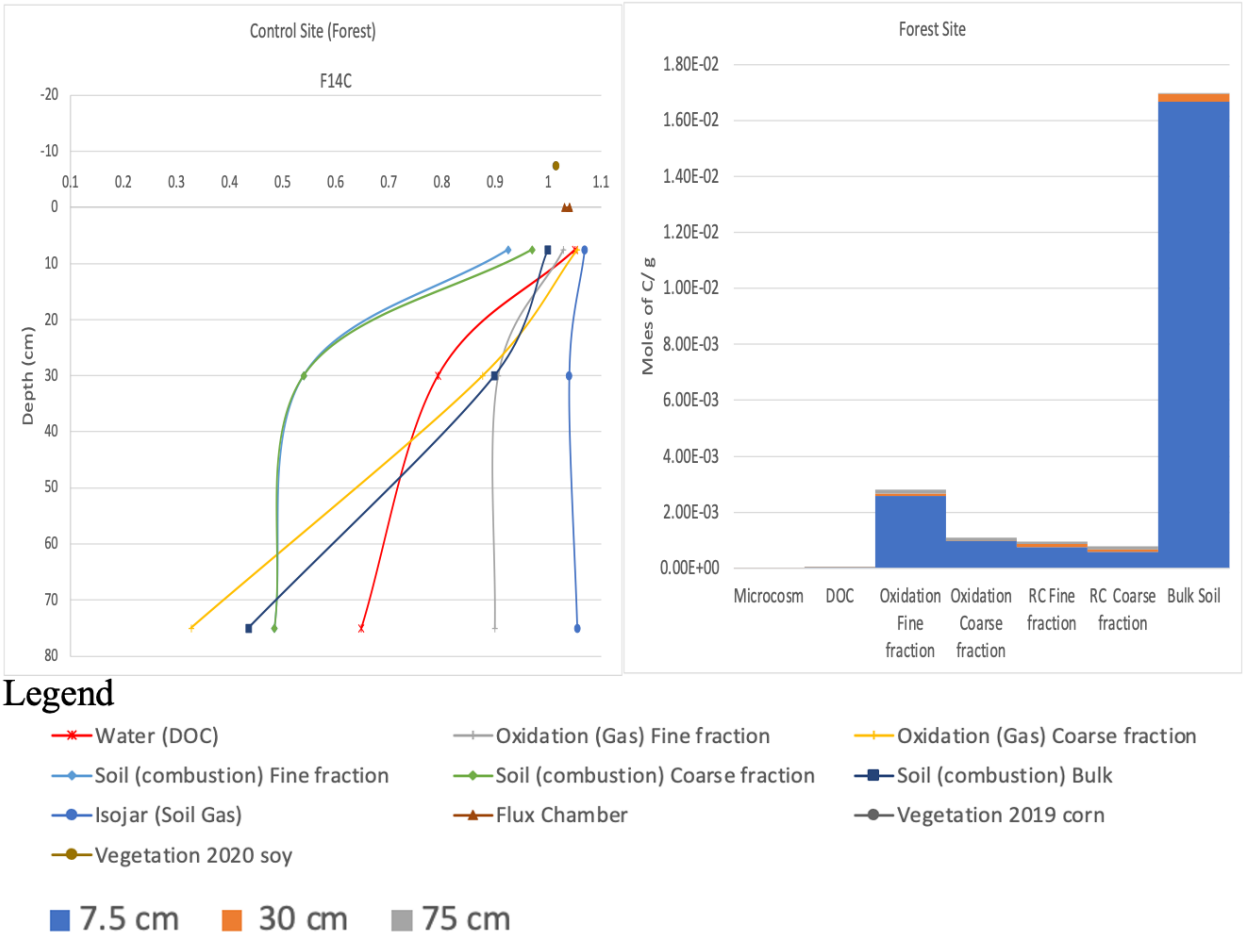

Figure 11. Carbon pool separation of Forest Control site was split into different carbon fractions: Liable fraction (DOC, Soil Gas), Organic Fraction (oxidizable fraction) and Recalcitrant fraction (soil combustion). The organic fraction and recalcitrant fractions were split respectively into a coarse fraction (greater than 60 microns) and fine fraction (0.45 microns to 60 microns). The figure on the right hand is displaying the mass of each fraction in comparison to the total bulk soil mass.

Figure 11 shows the carbon pool separation for the Control Site Forest, following the same procedure as for field site 1 (Figure 10). As shown again that the DOC in red, soil gas (Isojar) in blue and both oxidized fraction in yellow and gray are enriched in radiocarbon, whereas the combustion (recalcitrant) fractions in light blue and green are the primary factors that contribute to a lower Fm value. There is not much spread occurring at the depth of 7.5 cm, however we see a very significant spread occurring as depth increases. In addition, we see that the DOC fraction in red has a smaller Fm value than the fine and coarse grain oxidized fractions, which indicates that is has an older signature. This figure also demonstrates that the oxidized coarse grain fraction has a smaller Fm value than the anticipated Fm value of around 0.89 as the fine grain fraction displays and is closer to the combustion (recalcitrant) carbon for this sample (Rethemeyer et al., 2016). There is some variability for each of the elements that are shown in Figure 11. However, Figure 11 shows the same trend as seen in Figure 10. This indicates that even with some variability in the data, the data still demonstrate how each of these fractions contributes to the overall observable

radiocarbon signature when following each of them and comparing how they plot, in comparison to the bulk soil carbon. In both the field and background cores, the carbon pool that is being most accessible to microbial respiration throughout each profile, is observed in the IsoJar microcosms, which has the highest radiocarbon activity, and therefore is the most modern. Based on the data gathered for both Figures 10 and 11, we can determine that the DOC and the fine grain fraction (0.45 microns to 60 microns) are the fractions predominately used by microbial respiration. This is due to these individual fractions each having a very similar FM value to one another and this compares to the IsoJar (Soil Gas) fraction Fm value which follows the same trend as is observed in Figure's 10 and 11. Unlike the field site, which has been considerably worked, bulk soil carbon in the background site is less than about 200 years old, dominantly modern, and is dominated by the more labile pools measured in the oxidized step and with post-bomb fractions present at all depths.

Figure 12 presents the carbon-14 depth profile for the undredged study site 10. Field site 10 demonstrates that the microcosm profile in blue shows minor increases in age with depth. In addition, the Fm value stays above 1 up until a depth of 60 cm. This indicates that the carbon that is being used by microbial respiration is carbon deposited from the bomb pulse. The gas probes in both orange and grey are depleted in comparison to microcosms (Carsten et al., 2014). We can see that the gas probe in orange which was collected during a time when there was more moisture present in the soil profile, has more variation, in contrast to the grey probe which was collected during a period of low rain fall. We can clearly see the impact that carbonate weathering has on the soil gas that is respired on the Fm signature of these samples. In addition to observing the impact of carbonate weathering on the gas probes, the same impact is also seen in the gas flux chambers as these have a lower Fm value than the microcosms and are the cumulative gas that is being respired from the soil surface. As demonstrated in the graph, we can see that the gas probes and the flux chambers line up with one another showing the impact of carbonate weathering on them.

The carbon-14-depth profile for the Transition zone at site 10 is shown in Figure 12. The microcosm data show a very distinctive peak as depth increases, with all the values up to 75 cm having a Fm value greater than 1. This indicates that the carbon that is being used and transformed into CO_2 gas is originating from the bomb plus. As for the outlier that is seen in the microcosm profile, this can be attributed to having a very old carbon source present in the profile. When looking at the gas probe data it is seen that the gas probes are depleted in comparison to the microcosm. However, they display the same trend as the microcosm, and as previously mentioned, the depletion is attributed to carbonate weathering (Carsten et al., 2014). The gas flux chambers Fm values fall again between the gas probes and the microcosms which is to be expected, as the carbonate dissolution will impact the overall Fm value of the flux chambers. Finally, we can also see from the local vegetation, that the carbon being respired from these soils is originating from the bomb pulse due to the Fm signature decreasing back towards 1.

Radiocarbon Depth profile:

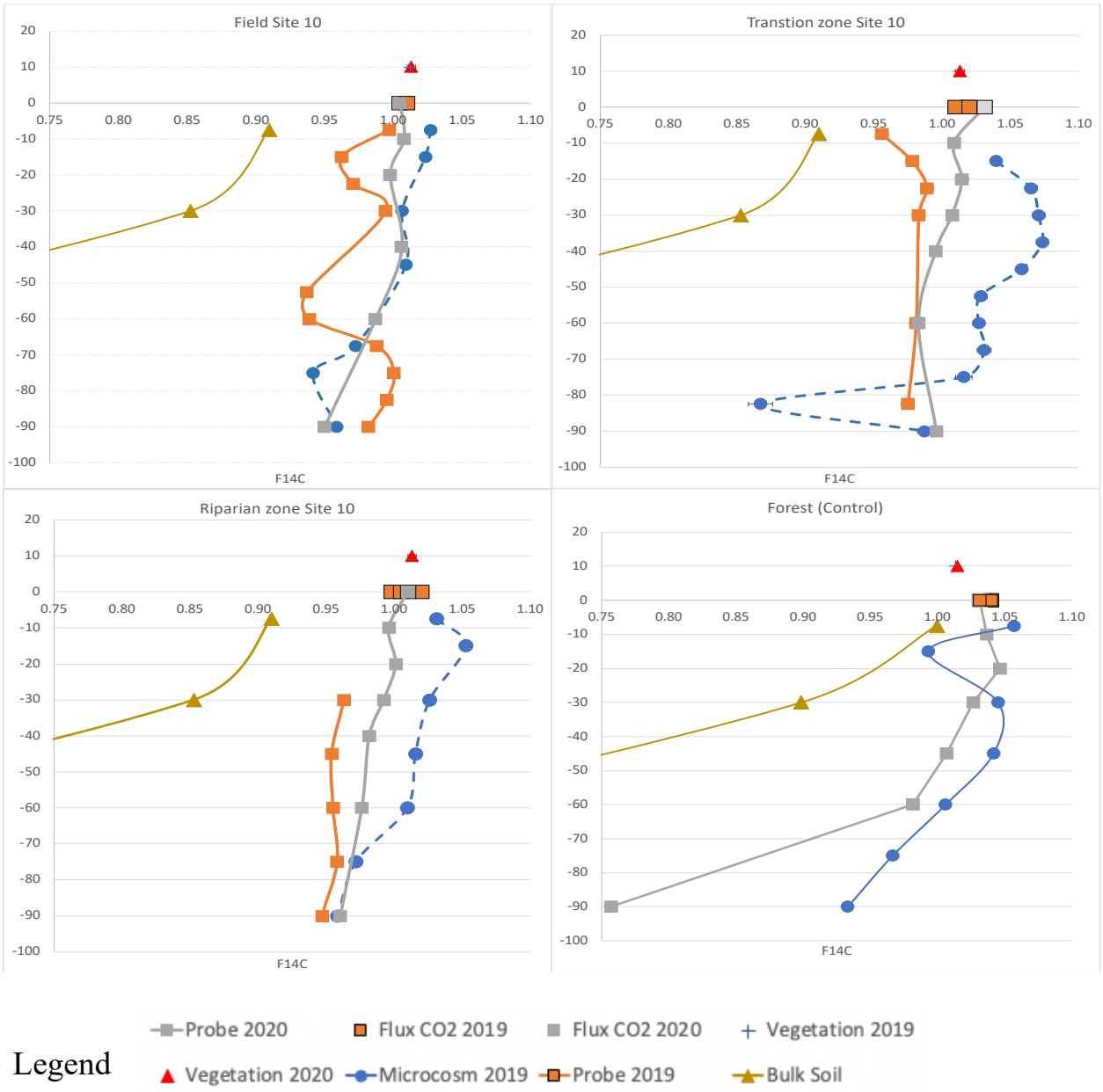

Figure 12. Carbon 14 depth profile for Study Site 10 microcosm, gas probes and gas flux chambers, including the control site forest. The riparian zone was not dredged the year prior to analysis.

The carbon-14-depth profile for the Riparian zone for the undredged site 10 is also shown in Figure 12. The microcosm data shows a clear peak in the soil profile at Fm value 1.05 but retains values greater than 1 down to a depth of greater than 60 cm. This indicates that respired labile organic carbon from the top of the profile up to 75 cm of depth is derived from the past several decades. In addition, the gas probe data demonstrates a similar trend as mentioned above, however they are being depleted in comparison to the microcosm signature. This same trend is also being demonstrated with the gas flux chambers. As previously mentioned, this is due to carbonate weathering causing a negative shift in the Fm values that are observed.

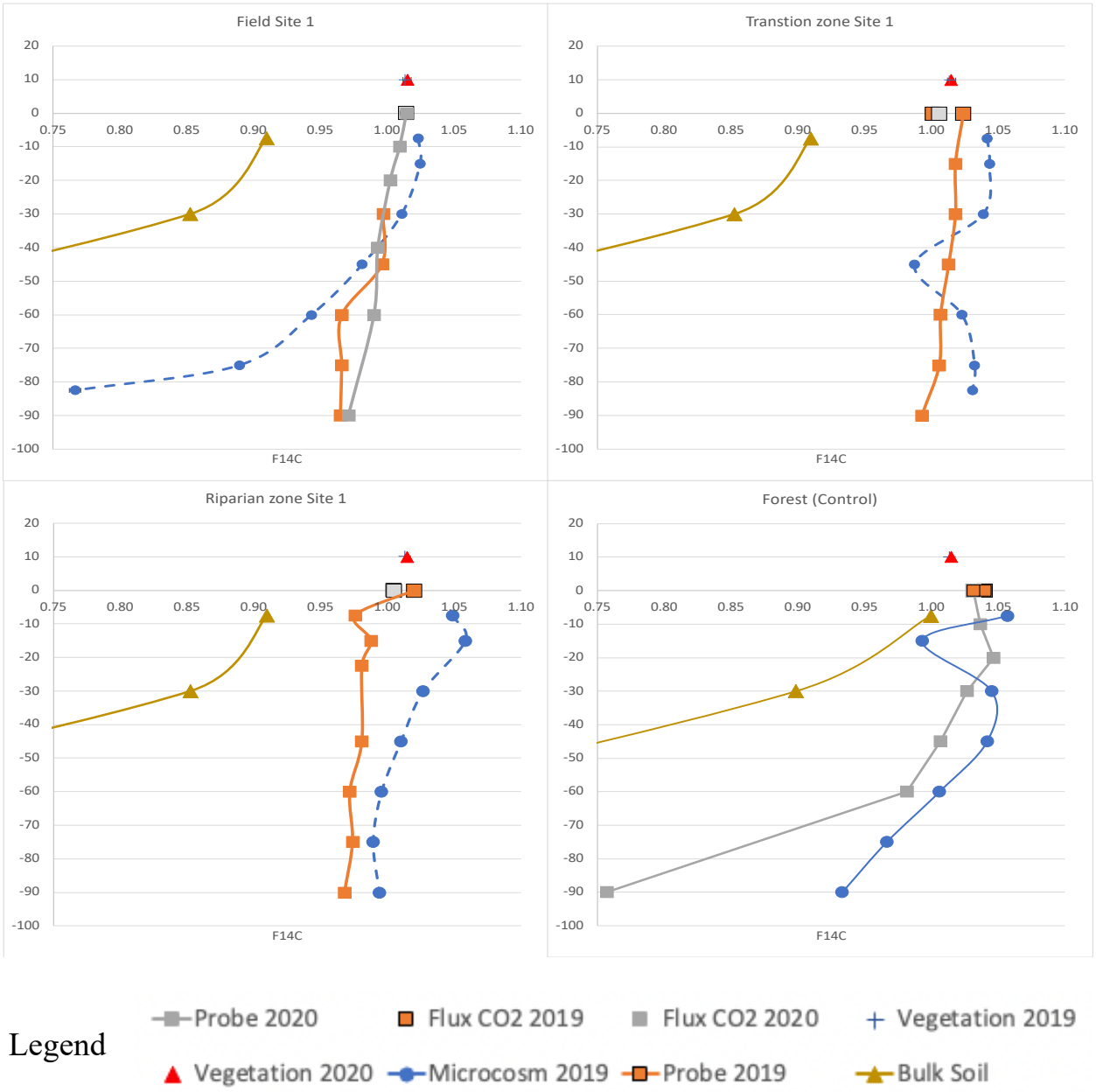

Figure 13. Carbon 14 depth profile for Study site 10 microcosm, gas probes and gas flux chambers, including the control site forest. The riparian zone was dredged the year prior to analysis.

Figure 13 depicts the carbon-14 depth profile for the dredged study site 1. The depth profile for field site 1, shows that the Fm values for the upper 30 cm are greater than 1, which is similar to field site 10. Below this depth, the microcosm profile deviates to considerably low Fm values, signifying respiration of carbon as old as 2300 years BP. The gas flux chamber CO_2 has a lower Fm value than the microcosm but a very similar signature to the gas probes, attributed to carbonate weathering in the profile. Unlike field site 1, the higher Fm at depth in field site 10 indicates that modern, labile carbon can be found at depth in these profiles. This can be attributed to tile drains

being installed in recent time, allowing for study site 10 to have a more homogeneous mixture when the soil was re-applied, whereas at site 1 this may not have occurred. In addition, we also have gas probe data, which in comparison to the microcosm profile, is slightly depleted and is attributed to carbonate weathering occurring in the soil, as observed with the ^{13}C data. Thus, for the shallow profile, these soils respire CO_2 gas from soil organic carbon dominated by bomb-pulse carbon dating from the past few decades.

The carbon-14-depth profile for the Transition zone at site 1 is also shown in Figure 13 for the dredged site. Both the microcosm profile and gas probe profile uniformly show Fm values greater than 1, indicating that organic carbon sequestered in the recent decades dominate to depth. However, when looking at the profile for this site, we can see that it is very uniform in comparison to the data displayed in study site 10 in Figure 12. The depth profile for both transition zones, that the observed Fm value of the CO_2 values is greater than those at the field sites for both study sites throughout the profile depicted in Figures 12 and 13. This occurrence of uniformly modern carbon throughout the profile is attributed to the emplacement of dredged soils (surface sediments and organics) from the ditch onto this transitional environment between the field and the dredged ditch.

The carbon-14-depth profile for the Riparian zone at site 1 is shown in Figure 13, which was dredged the year prior to sample collection. The microcosm depicts a clear peak in the shallow depth while for the rest of the profile, the Fm values do not drop to less than 0.99. The peak that is seen in the shallow depth of the microcosm is from an older carbon source, which we know to be the case because of the bomb pulse peak that slowly decreases. The gas probe is depleted in comparison to the microcosm, however, shows the exact same trend. As previously mentioned, this depletion is caused by carbonate weathering that is occurring in the soil profile. Looking at the local vegetation Fm value, we can see that it is in the middle of the other two measurements and that the carbon source from these two is younger than the carbon source that is found in the microcosms. When looking at the gas flux chambers, we see that these also fall in between the other two measurements, which is to be expected, as this is the overall gas that is being respired out of the soils. Finally, we can see a trend as we move from one location to the next at the same site, which indicates that in general the Fm values increase as you move to the riparian zone, suggesting that the carbon source at these locations is older in comparison to the field. Finally, when comparing both riparian zones from study site 10 and 1, they do not differ significantly and show the same trends for the age of the CO_2 that is being respired. After 1 year of vegetation re-growth, there is no significant impact on the age of the CO_2 gas that is being respired out of the soil.

Figures 12 and 13 both display the forest control site and the microcosm depth profile shows for the upper 30 post-modern values followed by a clear peak and then a decrease in the Fm values a depth increases. There is an outlier which is attributed to a root in that specific microcosm. However, the control site demonstrates the same trend as in the two riparian zones and transition zones; that young, post-bomb carbon dominates the upper profile, whereas the observed impact that the tilling has had on both the field sites, as their Fm values are lower in the upper section in comparison to the other locations and the background site. The impact from tilling is highest in the top 30 to 40 cm of the profile. However, organic carbon being respired back into the atmosphere is dominated by young carbon, despite the high amounts of old carbon sequestered in these profiles as seen in Figure 10. We see this trend in all the profiles where the microcosm Fm

value decreases with depth, however we do not see a drastic enough drop to indicate a significant decrease in age (Paul et al., 1997). Instead, see a rather uniform decrease in Fm value that would suggest that most of the organic carbon that is present in these soils is from the past 20 to 30 years in the upper 60 cm of the profiles. As such, we can also determine that microbes are using the most labile carbon that is present in the soils and therefore can infer that there is not much storing of carbon occurring at these sites specifically. This is further seen when comparing the soil carbon Fm values to the microcosm values as these follow the same trend but plot at different Fm values from one another indicating that the microbes are predominantly eating the more labile carbon fraction available.

Percent contribution of CO_2 gas weighted by Radiocarbon:

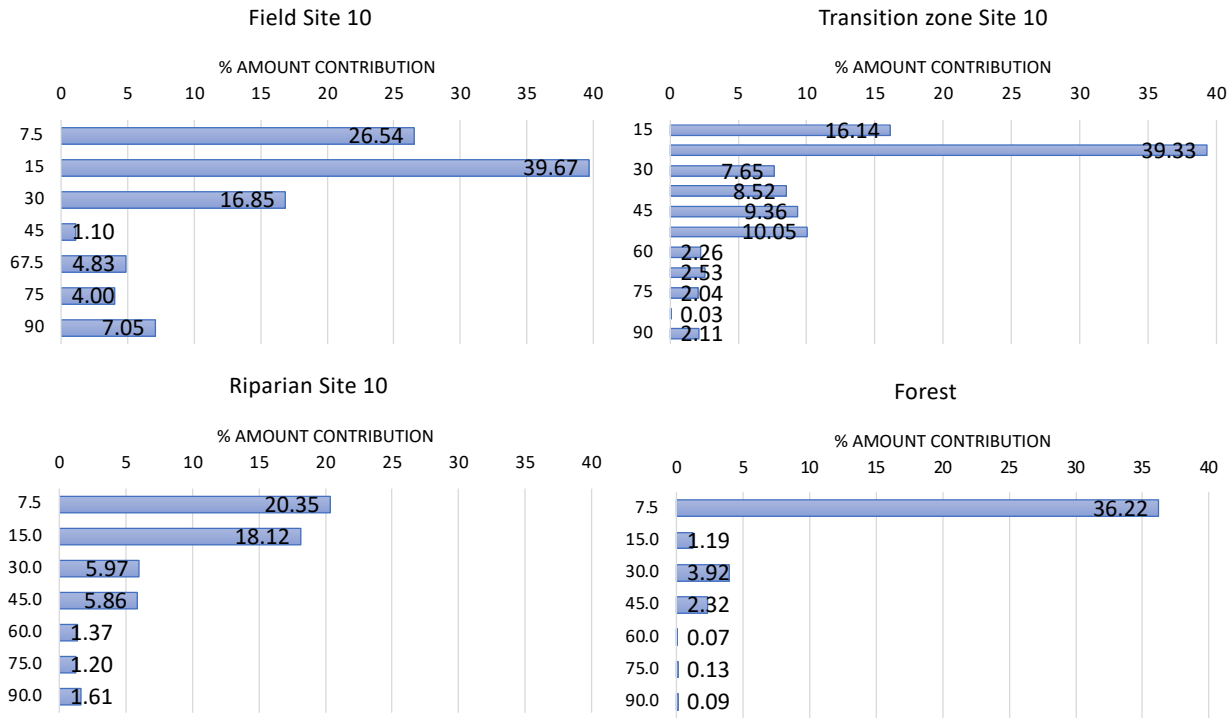

Figure 14. The overall percent contribution of each soil profile depth to the overall percent CO_2 emissions at the surface for study site 10 and the background site. Radiocarbon Fm values were used to calculate the overall percent contribution of each subsequent depth in the soil profile.

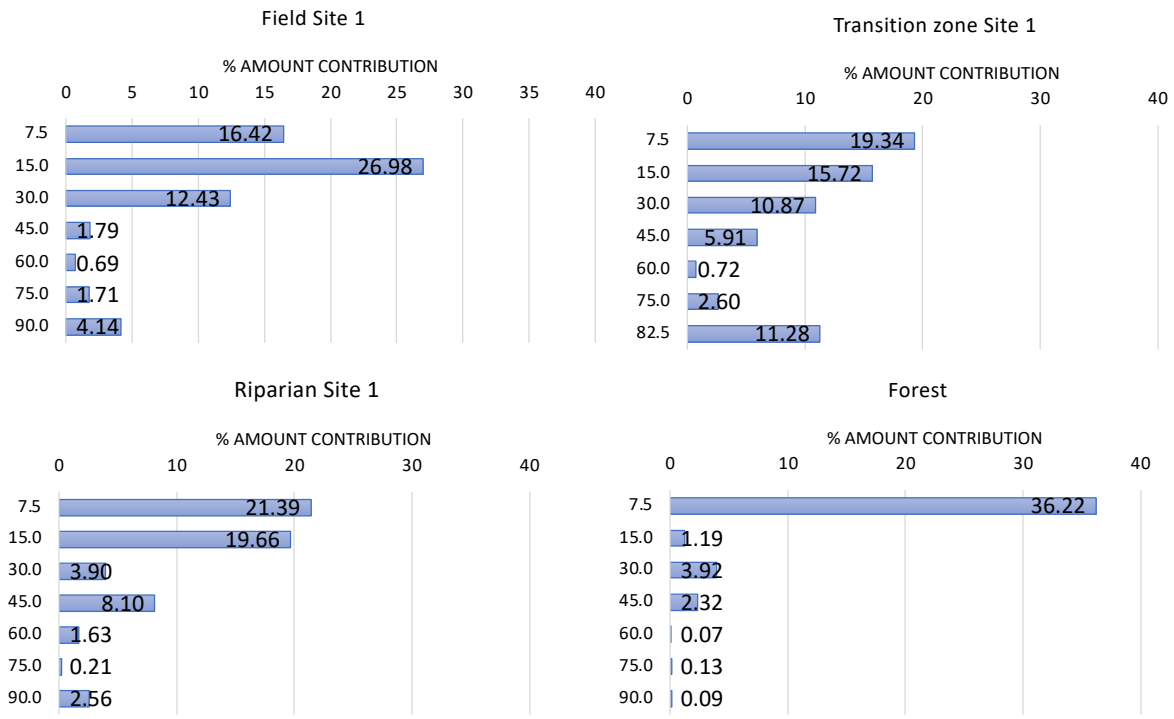

Figure 15. The overall percent contribution of each soil profile depth to the overall percent CO_2 emissions at the surface for study site 1 and the background site. Radiocarbon Fm values were used to calculate the overall percent contribution of each subsequent depth in the soil profile.

Figures 14 and 15 display the percent contribution of the microcosm CO_2 to the overall CO_2 signatures from the gas flux chambers for study sites 1 and 10. These are calculated from the rate of production data and to weighted by the Fm values of both the microcosm and the gas flux chambers to determine the percent contribution to the surface emissions. Figure 16 demonstrates that, apart from the dredged site 1 transition zone, the shallower depths (0-30 cm) contribute primarily to the overall radiocarbon signatures obtained from these soils. This also coincides with the data that was obtained in Figures 7 wherein we saw the highest rates of production in the shallowest depths. Interestingly to note, when looking at study site 1 we can see that at depth the percent contribution increases, which was similarly demonstrated at study site 10. However, the same trend is observed in Figure 7 which indicates that percent contribution is linked to the production rate of CO_2 and the soil organic carbon content.

Percent contribution of each size fraction to overall obtained fraction:

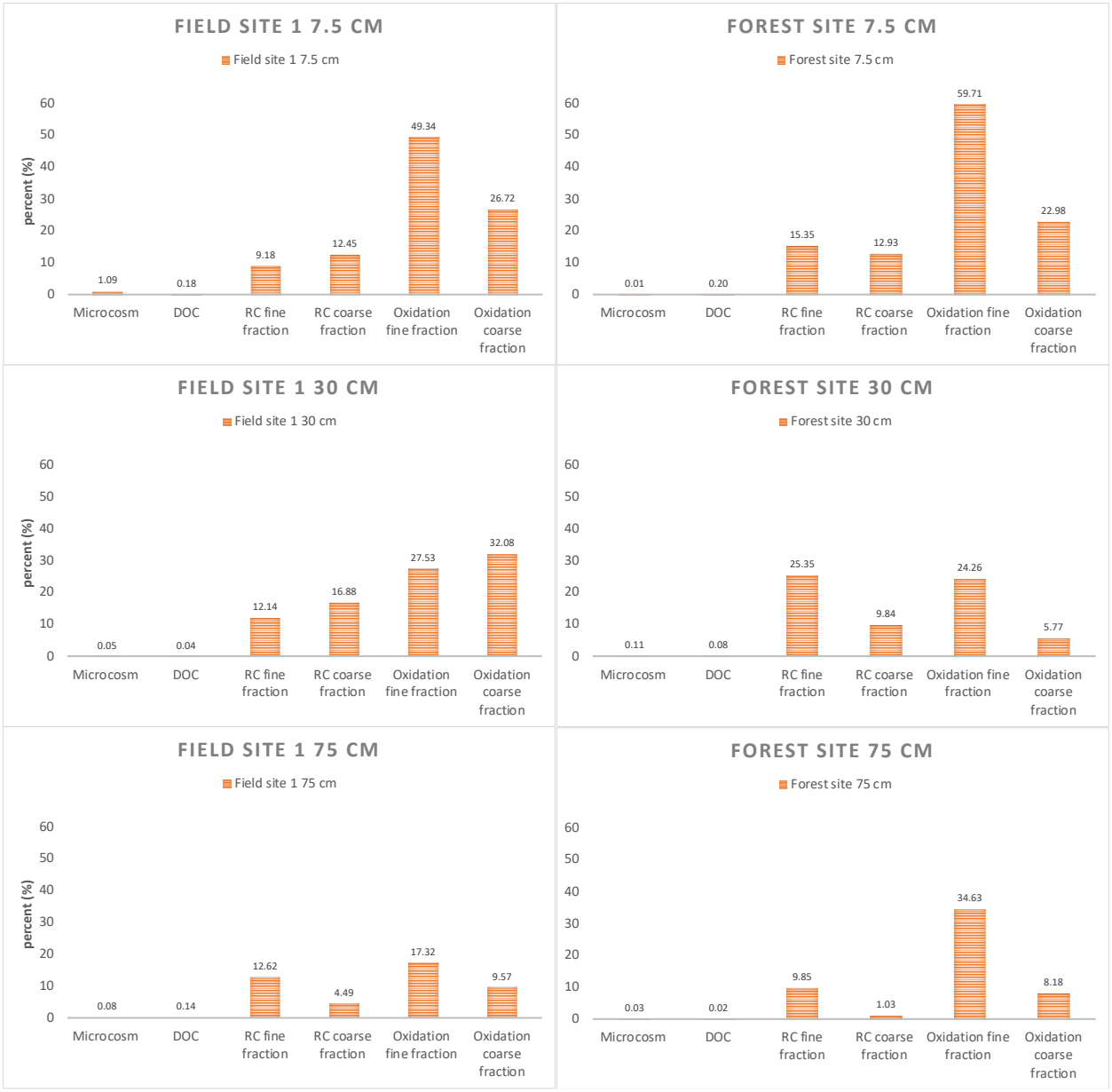

Figure 16. Carbon pool separation by size fraction and percent contribution of each invidual carbon pool.

Figure 16 displays the percent contribution of each carbon pool fraction to the radiocarbon content of the bulk soil for samples that were displayed in Figures 10 and 11. This figure begins at a shallow depth and progresses to a depth of 75 cm for both the field and background (forest) site. As depth increases, the field site on the left displays a decrease in the contribution from the soil organic carbon size fractions of 0.45-to-60-micron size while the remaining fractions increase. Additionally, for the field site, the recalcitrant fractions play a very significant role to the general contribution of the observed radiocarbon signatures. When comparing the field site to the control site, we see very similar trends which indicates that both sites behave very similarly. As previously mentioned, we see that the soil organic size fraction of 0.45-to-60-microns is the fraction that

contributes the most to the observed radiocarbon signature. However, this was unexpected as it was originally thought that the DOC fraction would be the fraction that would have the highest contribution of radiocarbon based on the perceived labile nature of DOC. What we can gather from this figure is that the soil organic fraction displays the highest contribution, followed by the recalcitrant fraction and finally the DOC and soil gas fractions. The microbes primarily use the organic carbon reservoir that is found in the soil for their metabolic processes. This indicates that most of the carbon stores in the soil is respired back out as CO_2 gas from the soils. This information better illustrates how the gas probes show a depleted signature in comparison to the microcosms, because the recalcitrant fraction has significant impact on the radiocarbon signatures that were obtained, and this, coupled with the carbonate weathering, would explain the depleted effect we observe in the gas probes (Zeng et al., 2020).

Mass balance using Radiocarbon:

Table 4. Mass balance of the carbon pool separation using Radiocarbon and the individual masses of labile carbon fraction, OC fraction and RC fraction.

Site	DOC labile fraction (g)	Organic fraction (g)	RC fraction (g)	Analytical value ($F^{14}C$)	Calculated value ($F^{14}C$)	Percent error %
Field Site 1 (7.5 cm)	0.0114	4.6087	1.6619	0.9097	0.8817	-3.08%
Field Site 1 (30 cm)	0.0029	4.5826	3.3179	0.8526	0.8062	-5.44%
Field Site 1 (75 cm)	0.0015	0.3179	0.5958	0.3741	0.4020	7.45%
Control (Forest 7.5 cm)	0.0362	15.4097	5.7762	0.9994	1.0112	1.18%
Control (Forest 30 cm)	0.0012	0.3824	0.8761	0.8986	0.5944	-33.85%
Control (Forest 75 cm)	0.0005	0.9893	0.7230	0.4351	0.4888	12.33%

Table 4 shows the mass balance for field site 1 and control site that were analyzed for carbon pool separation. The first column in Table 4 displays the mass of DOC labile fraction. In the subsequent column we have the mass of the organic fraction followed by mass of the recalcitrant (RC) fraction. In the fourth column of Table 4 we have the radiocarbon lab results followed by the value calculated by mass balance followed by the percent error of the method.

For the calculated values obtained from the radiocarbon standard decay equation, the percent error is below 10% for most of the values, which indicates that the method used for the carbon pool separation was successful. The control site at 30 cm has the largest percent error, and it is suspected that the presence of radiocarbon dead material may be the cause of this large error occurring, as this would cause the radiocarbon signature obtained to be significantly older. For the control site at 75 cm the error is only slightly over 10% and this may be due to the analysis that was performed to separate these different carbon pools which caused some modern contamination. As such, this would have affected samples that were more radiocarbon dead to have a higher error. Columns 1 to 3 demonstrate the masses for each carbon pool and we can see that throughout the three columns, the highest amount of organic carbon is present in the organic fraction, followed by the RC

fraction, and finally the DOC fraction. However, the control site forest at 30 cm has an anomaly in the amount of carbon present in the organic fraction, which is most likely imparts the high error for that specific depth. Finally, these three columns also line up with that observed in Figure 16 with the percent contributions of each carbon pool fraction. Table 4 shows that carbon pool separation worked, and that the method used to separate these different carbon pools did not result in significant error throughout the analysis.

Summary

The three sites in each cross section included the farmed field, and the associated riparian zone with a dredged ditch and a transition site in the middle near the field edge where dredged material in the past was deposited. Site 1 was dredged most recently in 2018 whereas Site 10, located 2 km north was left undredged in that year for the purposes of this research program.

Rate of CO_2 production vs Organic carbon content

Figure's 6 and 7 shows the rate of CO_2 production graphed with organic carbon content of the soils. In general, high organic carbon content samples have a high rate of production, although some anomalies exist. The carbon content and CO_2 production are much higher in the undredged (Site 10) riparian and transition zones. In contrast, both field sites have similar organic carbon content and production rates, which decrease rapidly below the plow depth of 30 cm. The background (forested) site shows the lowest CO_2 production rates and organic carbon at all depths except for the top (7.5 cm), which is presumably contributions from leaf litter. These data help better evaluate which depths in these depth profiles are the most active and contribute more to the overall respiration of CO_2. We can infer that we would detect younger CO_2 (CO_2 from the bomb pulse) in the shallow depths and observe an older CO_2 signature at depth.

^{13}C and Radiocarbon

The ^{13}C stable isotope data provided us with several points of information, in particular what carbon source was present at each of these sites and a clear indication that carbonate weathering was occurring in the system. The data displayed in Figure's 8 and 9 showed that the primary type of carbon that is present originates from C3 plants throughout the depth profiles at all study locations. When there was presence of C4 plant carbon in the depth profile, it was only during the 2019 season in which corn (C4 plant) was grown, indicating that these only had a seasonal effect on the type of carbon present. Only in field site 10 for 2019, was soil probe samples below 60 cm, displaying a strong C4 signature. This is matched with an enrichment to modern values for ^{14}C, suggesting macropore transport (likely worm holes) of root-respired CO_2 to that section.

The gas probe data displayed a very interesting anomaly across all sites that were sampled, which depicted that this data was enriched in ^{13}C and depleted in $F^{14}C$ in comparison to the microcosm signatures that were obtained. This is attributed to carbonate weathering and dissolution. The data that was obtained from the gas probe data for both years 2019 and 2020, showed that the gas probes at both sites were enriched in comparison to the soil organic ^{13}C signature and microcosm ^{13}C. These enrichments are accompanied by a depletion in ^{14}C relative to the microcosms, as observed for all transects at both sites 1 and 10. This enrichment in ^{13}C and depletion in ^{14}C, relative to microcosm CO_2 samples, likely indicates minor weathering of the low carbonate content of the soils contributing marine carbon to the CO_2 ($\delta^{13}C = 0‰$; $F^{14}C = 0$). Therefore, this overall observation cannot be attributed to contributions from C4 plants. This same enrichment was also seen in the gas flux chambers, showing consistency between subsurface gases and surface emissions. It is important to note the effect of this weathering and contribution of carbonate CO_2 to the in-situ soil gases on the estimation of radiocarbon ages.

All profiles in Figure's 12 and 13 show an overall trend towards lower ^{14}C activities with depth. The shallow data (to 40 cm) for the field sites show that tilling at the field site had a significant impact on the isotopic data that was obtained at these locations. Comparing the three different locations at each site, it is evident that carbon in the field sites (Figure's 6 and 7) was not as well preserved as in the other two locations. This was evident when looking at the $F^{14}C$ signatures for the microcosms of each location, which show little preservation of bomb-pulse carbon from recent decades. This further demonstrates the impact tilling has on these soils for carbon recycling. This further indicates that worked plots of land are not good at preserving carbon. Microcosm values in the top 40 cm of the soil profile depict that the CO_2 has residual carbon from the bomb pulse.

In addition, the probe data in the field sites closely align to the ^{14}C value of modern vegetation. With a nominal correction for marine carbonate in the probe data, this suggests that the surface emissions are enriched by 2 to 3 permil and therefore are dominated by respiration of carbon which is 2 to 3 years old (note from above that atmospheric $^{14}CO_2$ decreases by about 1 permil per year). The carbon in the subsequent depths from 30 cm to around 60 cm at both Riparian sites, Transition zone and Control site still showed radiocarbon values that link it to the bomb pulse whereas others displayed a slightly older source. At depths greater than 60 cm, all had carbon that originated prior to the 1950s. In particular, the microcosm radiocarbon profile for field sites 1 and 10 decreased with depth to values below 0.95 Fm, demonstrating respiration of old carbon. These correlate with data from Figure's 6 and 7, showing that these samples have a very low production rate from very low carbon content.

Radiocarbon profiles for the forest background site showed enrichments in ^{14}C above 1.00 down to a depth of 60 cm for both the soil probe samples and the microcosms, which contrasted with the field data where this transition occurred at a shallower depth. This suggests that carbon sequestration and cycling occurred through a deeper profile for the forested site than for the tilled fields, perhaps due to the greater depth of root penetration. Finally, the same trend is observed at riparian site 10, which suggests that carbon sequestration and cycling occurs through a deeper profile as in the forested site.

Comparison of the dredged (Site 1) versus undredged (Site 10) riparian microcosm $^{14}CO_2$ profiles showed remarkably little impact of dredging on the age structure of carbon sequestered in these soil profiles. Both have similar profiles to that of the forest background site in that they have modern (post-bomb) carbon down to a depth of 60 cm. In contrast, the transition zone in both Sites 1 and 10 have post-bomb carbon through most of their profile, likely reflecting the deposition of dredged material in the current experiment (2019) and in the recent past (1980s). Finally, from this data we can infer that after 1 year post dredging there is no significant impact on the age of CO_2 gas that is being respired out the soil from the dredged (Site 1) versus the undredged (Site 10).

Carbon pool separation

The data that was obtained from the carbon pool separation provided an age structure to the different carbon pools. This data then demonstrated which fractions had the strongest influence overall on the microcosm emissions. Bulk carbon in the field site varied from several hundred years to late Holocene in age. The carbon fraction that contributed the greatest mass in each of these profiles was the oxidized fraction. In addition, each of these different fractions were separated by size and yielded additional information into which fraction was truly contributing the majority of organic carbon; between 0.45 – 60 microns. This was further perceived when performing the mass balance method and graphing the percent contributions, as seen in Figure 16. This data indicated that the carbon source that was being used for the microbial respiration was coming primarily from the size fraction of 0.45 – 60 microns and that the other fractions contributed minorly to the overall fraction. Finally, with this information, a mass balance was able to be performed for two of these sites. The results from this mass balance were quite promising as they indicated that the method used for the separation of the carbon pools was effective. Further studies should be conducted to better understand the impact of each carbon pool and to see how separating each fraction by size impacts the radiocarbon signatures observed.

General Conclusions

This research focused on the age of CO_2 emissions from soils in agricultural fields and associated riparian zones that were subjected to dredging.

Soil organic carbon has radiocarbon age ranges from modern to late Pleistocene, but mostly late Holocene. Specific depths show that different carbon fractions have different ages; the more labile (oxidizable) carbon is youngest. Size fractionation showed comparatively less variation in ages. The recalcitrant carbon pool in all samples that survived the oxidation step in these experiments was uniformly the oldest. Dating of carbon fractions also showed that at greater depth, organic carbon was older and at all depths below 30 cm was deposited prior to the testing of nuclear bombs, as seen in the fraction from the microcosm samples.

These microcosm experiments were effective in showing that the age of respired CO_2 is considerably younger than the bulk age of soil carbon. Additionally, that the top 30 cm of the soil profile the CO_2 gas that was being respired largely originated from the bomb pulse, and so is on the order of decades old. Therefore, heterotrophic activity selectively respires young and presumably more labile carbon sources within the heterogeneous mix of soil carbon. It is understood that these ages are a weighted mean of a range of ages in the labile organic carbon.

The microcosm experiments show that post-bomb, ^{14}C-enriched labile carbon dominates throughout the profiles in the riparian and transition sites, but only in the shallower profile (to the 30 cm plow pan) at the field sites at both undredged and dredged sites. Therefore, there is a greater reservoir of decades-old carbon in the transition and riparian sites than in the fields. The fields have younger carbon in this shallow depth (years to decade) and therefore recycle carbon more rapidly, likely due to plowing.

Carbonate weathering by carbonic acid was observed in the soil gas probe data, but not in the microcosm data, giving similar but marginally depleted ^{14}C trends due to contributions of ancient marine carbonate. These observations were supported by the stable isotope data, where the soil probe CO_2 data was enriched in ^{13}C relative to the microcosm data. CO_2 in surface emissions and soil probes therefore have older apparent ages due to this incorporation of inorganic carbon from carbonate weathering.

The surface flux chamber data for ^{13}C and ^{14}C coincide, with some seasonal variability, with the extrapolation to surface of the shallow (<30 cm soil probe CO_2 profiles), demonstrating a clear link between shallow, in-situ production of CO_2 and surface emissions. This allows the age determination of these emissions, corrected for carbonate dissolution in the soils using the microcosm CO_2 data for the shallow soil.

The comparison of the dredged and undredged sites suggests little difference in the ages or rates of emissions from these contrasting sites. However, there are strong differences between the riparian/transition sites and the field sites in this agricultural landscape.

Radiocarbon measurements of CO_2 from surface flux chambers from soil probes together with production and ^{14}C of CO_2 in microcosm experiments, provide a valuable approach to assessing the source and age of emissions from terrestrial landscapes.

References

Cornelius Adewale, John P. Reganold, Stewart Higgins, R. Dave Evans, Lynne Carpenter-Boggs, Agricultural carbon footprint is farm specific: Case study of two organic farms, Journal of Cleaner Production, Volume 229, 2019, Pages 795-805, ISSN 0959-6526, https://doi.org/10.1016/j.jclepro.2019.04.253.

Verónica Berriel, Carlos Perdomo, Determination of high fructose corn syrup concentration in Uruguayan honey by ^{13}C analyses, LWT, Volume 73, 2016, Pages 649-653, ISSN 0023-6438, https://doi.org/10.1016/j.lwt.2016.07.004.

Bernhard Ahrens, Maarten C. Braakhekke, Georg Guggenberger, Marion Schrumpf, Markus Reichstein, Contribution of sorption, DOC transport and microbial interactions to the ^{14}C age of a soil organic carbon profile: Insights from a calibrated process model, Soil Biology and Biochemistry, Volume 88, 2015, Pages 390-402, ISSN 0038-0717, https://doi.org/10.1016/j.soilbio.2015.06.008.

Blume, O., Guitard, E., Crann, C., Orekhov, M., Amos, R., Clark, I., Lapen, D., Blowes, D., Ptacek, C., Craiovan, E., & Sunohara, M. (2022). Relationships between carbon age and CO_2 efflux in agricultural and drainage ditch soils using the thermonuclear bomb pulse. Vadose Zone Journal, e20208. https://doi.org/10.1002/vzj2.20208

Roberto Alvarez, Raúl A. Díaz, Nidia Barbero, Oscar J. Santanatoglia, Luis Blotta, Soil organic carbon, microbial biomass and CO_2-C production from three tillage systems, Soil and Tillage Research, Volume 33, Issue 1, 1995, Pages 17-28, ISSN 0167-1987, https://doi.org/10.1016/0167-1987(94)00432-E.

Ball, B.C. (2013), Soil structure and greenhouse gas emissions: a synthesis of 20 years of experimentation. Eur J Soil Sci, 64: 357-373. https://doi.org/10.1111/ejss.12013

Peter E. Carlson, Jay L. Banner, Kathleen R. Johnson, Richard C. Casteel, Daniel O. Breecker, Carbon cycling of subsurface organic matter recorded in speleothem ^{14}C records: Maximizing bomb-peak model fidelity, Geochimica et Cosmochimica Acta, Volume 246, 2019, Pages 436-449, ISSN 0016-7037, https://doi.org/10.1016/j.gca.2018.11.035.

Clark, I. (2015). Groundwater geochemistry and isotopes (1st ed.). CRC Press. https://doi.org/10.1201/b18347

Cui, Z.L. , S.C. Yue, G.L. Wang, F.S. Zhang, X.P. Chen
In-season root-zone N management for mitigating greenhouse gas emission and reactive N losses in intensive wheat production Environ. Sci. Technol., 47 (2013), pp. 6015-6022, 10.1021/es4003026

Doner, L.W. , J.W. White Jr. Carbon-13/- ratio is relatively uniform among honeys Science, 197 (1977), pp. 891-892

Don, A., Schumacher, J. and Freibauer, A. (2011), Impact of tropical land-use change on soil organic carbon stocks – a meta-analysis. Global Change Biology, 17: 1658-1670. https://doi.org/10.1111/j.1365-2486.2010.02336.x

Follett, Ronald F.1; Paul, Eldor A.2; Pruessner, Elizabeth G.1. SOIL CARBON DYNAMICS DURING A LONG-TERM INCUBATION STUDY INVOLVING 13C AND 14C MEASUREMENTS. Soil Science 172(3):p 189-208, March 2007. | DOI: 10.1097/ss.0b013e31803403de

Government of Canada, (2019). Description of soil ONBIVSS~~~A (BAINSVILLE). Retrieved from https://sis.agr.gc.ca/cansis/soils/on/BIV/O~~~~/N/description.html

Government of Canada Agriculture and Agri-Food Canada (AAFC), Evaluation of the Agricultural Greenhouse Gases Program (2016-17 to 2020-21) – Summary, (2021-03-18)

Hartemink, A.E., The depiction of soil profiles since the late 1700s, CATENA, Volume 79, Issue 2, 2009, Pages 113-127, ISSN 0341-8162, https://doi.org/10.1016/j.catena.2009.06.002.

Hua, Q., Barbetti, M., & Rakowski, A. (2013). Atmospheric Radiocarbon for the Period 1950–2010. Radiocarbon, 55(4), 2059-2072. doi:10.2458/azu_js_rc.v55i2.16177

Wang, Haiyan, Jiangqi Wu, Guang Li, Lijuan Yan, Shuainan Liu,
Effects of extreme rainfall frequency on soil organic carbon fractions and carbon pool in a wet meadow on the Qinghai-Tibet Plateau, Ecological Indicators, Volume 146, 2023, 109853, ISSN 1470-160X, https://doi.org/10.1016/j.ecolind.2022.109853.

Janzen, H.H., Carbon cycling in earth systems—a soil science perspective,
Agriculture, Ecosystems & Environment, Volume 104, Issue 3, 2004, Pages 399-417,
ISSN 0167-8809, https://doi.org/10.1016/j.agee.2004.01.040.

Jobbagy, Esteban G., and Robert B. Jackson. “The Vertical Distribution of Soil Organic Carbon and Its Relation to Climate and Vegetation.” Ecological Applications, vol. 10, no. 2, 2000, pp. 423–36. JSTOR, https://doi.org/10.2307/2641104

Lal, R., W. Negassa, K. Lorenz Carbon sequestration in soil Current Opinion in Environmental Sustainability, Environmental change issues, vol. 15 (2015), pp. 79-86
https://doi.org/10.1016/j.cosust.2015.09.002

Orekhov, Michel, Radiocarbon Analysis in Soils from Agricultural fields to Trace CO_2 Emissions, (2017), University of Ottawa

Paul, E.A., Follett, R.F., Leavitt, S.W., Halvorson, A., Peterson, G.A. and Lyon, D.J. (1997), Radiocarbon Dating for Determination of Soil Organic Matter Pool Sizes and Dynamics. Soil Science Society of America Journal, 61: 1058-
1067. https://doi.org/10.2136/sssaj1997.03615995006100040011x

Poeplau, C. , A. Don, 2015. Carbon sequestration in agricultural soils via cultivation of cover crops – a meta-analysis Agric. Ecosyst. Environ., 200 (2015), pp. 33-41 https://doi.org/10.1016/j.agee.2014.10.024

Poeplau Christopher, Axel Don, Carbon sequestration in agricultural soils via cultivation of cover crops – A meta-analysis, Agriculture, Ecosystems & Environment, Volume 200, 2015, Pages 33-41, ISSN 0167-8809, https://doi.org/10.1016/j.agee.2014.10.024.

van der Plicht, J., H.J. Streurman, J.M. van Mourik, Chapter 3 - Radiocarbon dating of soil archives, Editor(s): Jan M. Van Mourik, Jaap J.M. Van Der Meer, Developments in Quaternary Sciences, Elsevier, Volume 18, 2019, Pages 81-113, https://doi.org/10.1016/B978-0-444-64108-3.00003-3.

Rethemeyer, J., Kramer, C., Gleixner, G., Wiesenberg, G., Schwark, L., Andersen, N., Grootes, P. (2004). Complexity of Soil Organic Matter: AMS 14C Analysis of Soil Lipid Fractions and Individual Compounds. Radiocarbon, 46(1), 465-473. doi:10.1017/S0033822200039771

Rehman, Abdul, Mohammad Mahtab Alam, Rafael Alvarado, Cem Işık, Fayyaz Ahmad, Laura Mariana Cismas, Mariana Claudia Mungiu Pupazan, Carbonization and agricultural productivity in Bhutan: Investigating the impact of crops production, fertilizer usage, and employment on CO2 emissions, Journal of Cleaner Production, Volume 375, 2022, 134178, ISSN 0959-6526, https://doi.org/10.1016/j.jclepro.2022.134178.

Slessarev, Eric W. , Erin E. Nuccio, Karis J. McFarlane, Christina E. Ramon, Malay Saha, Mary K. Firestone, Jennifer Pett-Ridge Quantifying the effects of switchgrass (Panicum virgatum) on deep organic C stocks using natural abundance 14C in three marginal soils First published: 19 July 2020 https://doi.org/10.1111/gcbb.12729

Shi, Z., Allison, S.D., He, Y. et al. The age distribution of global soil carbon inferred from radiocarbon measurements. Nat. Geosci. 13, 555–559 (2020). https://doi.org/10.1038/s41561-020-0596-z

Liu, Xuyang, Weiqi Wang, Josep Peñuelas, Jordi Sardans, Xiaoxuan Chen, Yunying Fang, Abdulwahed Fahad Alrefaei, Fanjiang Zeng, Akash Tariq,
Effects of nitrogen-enriched biochar on subtropical paddy soil organic carbon pool dynamics, Science of The Total Environment, Volume 851, Part 2, 2022, 158322, ISSN 0048-9697, https://doi.org/10.1016/j.scitotenv.2022.158322.

Du, Xuejun, Zijun Xu, Qilin Lv, Yunshan Meng, Zihe Wang, Haojie Feng, Xueqin Ren, Shuwen Hu, Zideng Gao, Fractions, stability, and influencing factors of soil organic carbon under different land-use in sodic soils, Geoderma Regional, Volume 31, 2022, e00590, ISSN 2352-0094, https://doi.org/10.1016/j.geodrs.2022.e00590.

C.Q. Yu, X. Huang, H. Chen, H.C.J.Godfray, J.S. Wright, J.W. Hall, P. Gong, S.Q. Ni, S.C. Qiao , G.R. Huang, Y.C. Xiao, J. Zhang, Z. Feng, X.T. Ju, P. Ciais, N.C.Stenseth, D.O. Hessen, Z.L. S un, L. Yu, W.J. Cai, H.H. Fu, X.M. Huang, C. Zhang, H.B. Liu, J. Taylor
Managing nitrogen to restore water quality in China
Nature, 567 (2019), pp. 516-520, 10.1038/s41586-019-1001-1

Zhang, Wushuai, Yuan Qiao, Prakash Lakshmanan, Liuzheng Yuan, Jiayou Liu, Chenghu Zhong, Xinping Chen, 2022. Combing public-private partnership and large-scale farming increased net ecosystem carbon budget and reduced carbon footprint of maize production, Resources, Conservation and Recycling, Volume 184, 2022, 106411, ISSN 0921-3449, https://doi.org/10.1016/j.resconrec.2022.106411.

Wicklund, R. E., & Richards, N. R. (1962). Soil Survey of Russell and Prescott Counties. Ontario Soil Survey, (33).

Zeng, Sibo, Zaihua Liu, Chris Groves,
Large-scale CO2 removal by enhanced carbonate weathering from changes in land-use practices, Earth-Science Reviews, Volume 225, 2022, 103915, ISSN 0012-8252, https://doi.org/10.1016/j.earscirev.2021.103915.

Zimmermann, M., J. Leifeld, J. Fuhrer,
Quantifying soil organic carbon fractions by infrared-spectroscopy,
Soil Biology and Biochemistry, Volume 39, Issue 1, 2007, Pages 224-231, ISSN 0038-0717, https://doi.org/10.1016/j.soilbio.2006.07.010.